PERGAMON

International Journal of Solids and Structures 36 (1999) 4111–4147

INTERNATIONAL JOURNAL OF SOLIDS and STRUCTURES

# Non-linear response of laminated plates and shells to thermomechanical loading: Implications of violation of interlaminar shear traction continuity requirement

Liviu Librescu*, Weiqing Lin

*Department of Engineering Science and Mechanics, Virginia Polytechnic Institute and State University, Blacksburg, VA 24061-0219, U.S.A.*

Received 4 January 1998; in revised form 13 May 1998

**Abstract**

A number of results focusing on the implications brought by the violation of the inter-laminar shear traction continuity requirement on the non-linear response of shear deformable laminated flat and curved panels subjected to thermomechanical loading are presented. The results cover a large number of situations, and in this context, the effects of transverse shear, tangential edge constraints, shell curvature, initial geometric imperfections, lateral pressure and compressive edge loads, membrane and thicknesswise temperature gradient, presence of a Winkler linear/non-linear foundation, coupled with that of the fulfilment/violation of the shear traction interlaminar continuity requirement upon the static and dynamic non-linear response of laminated plates and shells are highlighted. In order to address this problem, as a necessary pre-requisite, a higher-order geometrically non-linear laminated shell model fulfilling both the kinematical and shear traction interlaminar continuity requirements and incorporating the previously mentioned effects is presented. The results obtained in the framework of this laminated shell model are compared with the ones obtained within a higher-order shell model in which the kinematic interlaminar continuity conditions are solely satisfied, and the implications resulting from the violation of the shear traction interlaminar continuity requirement are highlighted. 

## Nomenclature

| | |
|---|---|
| $a_{\alpha\beta}$, $a^{\alpha\beta}$ | covariant and contravariant components of the metric tensor of the undeformed mid-surface $\sigma$ |
| $\mathscr{T}$, $\mathscr{L}$, $\mathscr{S}$, $\mathscr{K}$, $\tilde{b}$, $\tilde{c}$ | stiffness quantities |
| $b_{\alpha\beta}$ | curvature tensor of the undeformed mid-surface |
| $b_{11}(\equiv 1/R_1)$; $b_{22}(\equiv 1/R_2)$ | principal curvatures of $\sigma$ |
| $c^{\alpha\beta}$ | 2-D permutation symbol |

* Corresponding author. Tel.: 001 540 231 5916; Fax: 001 540 231 4574; E-mail: librescu@vt.edu

0020–7683/99/$ - see front matter 
PII: S0020–7683(98)00185–1

| | |
|---|---|
| $\mathscr{D}$ | flexural stiffness |
| $e_{\alpha\beta}$, $e_{\alpha 3}$ | 3-D tangential and transverse shear strain components |
| $E$, $E'$ | Young's modulus, tangential and transversal to the isotropy surface |
| $E^{ijrs}$, $F_{ijrs}$ | tensor of elastic coefficients and the compliance elastic tensor, respectively |
| $f(x^3)$ | function characterizing the variation of $\sigma^{\alpha 3}$ in the thickness direction |
| $w_{mn}$, $\mathring{w}_{mn}$ | amplitudes in the mode $(m, n)$ of $v_3$, $\mathring{v}_3$ |
| $F_\omega(x^\alpha)$ | functions defining the tangential variation of $\sigma^{\alpha 3}$ |
| $G$, $G'$ | tangential and transverse shear modulus, respectively |
| $h$ | total thickness of shell/plate |
| $H$ | mean curvature of $\sigma$ |
| $K^2$ | transverse shear correction factor |
| $\bar{K}_1$, $\bar{K}_3$, $(K_1, K_3)$ | linear and cubic Winkler's foundation moduli (their dimensionless counterparts) |
| $l_1$, $l_2$ | length and width of the flat/curved panel |
| $L_{11}$, $L_{22}$ | dimensionless compressive edge loads, positive in compression $(\equiv(\mathscr{N}_{11}, \mathscr{N}_{22})l_1^2/\pi^4\mathscr{D})$ |
| $L_R$ | edge load ratio $L_{22}/L_{11}(\equiv\mathscr{N}_{22}/\mathscr{N}_{11})$ |
| $\mathscr{N}_{11}$, $\mathscr{N}_{22}$ | edge loads normal to the edges $x_1 = 0$, $l_1$ and $x_2 = 0$, $l_2$, respectively, positive in compression |
| $N^{\alpha\beta}$, $M^{\alpha\beta}$, $Q^{\alpha 3}$ | tensors of stress resultants, stress couples and transverse shear stress resultant, respectively |
| $p_3$, $p_{mn}$, $\hat{p}(\equiv p_{11}l_1^4/(\mathscr{D}h))$ | lateral pressure field, and its amplitude in the mode $(m, n)$ and the dimensionless amplitude in the mode (1, 1), respectively |
| $S_{ij}$ | second Piola–Kirchhoff stress tensor |
| $t_c$, $t_f$ | thickness of the core and of upper or bottom facings, respectively |
| $t$ | time variable |
| $\overset{\circ}{T}(x^\alpha)$, $\overset{1}{T}(x^\alpha)$ | membrane and thicknesswise temperature distributions |
| $\overset{\circ}{T}_{mn}$, $\overset{1}{T}_{mn}$ | amplitudes in the mode $(m, n)$ of $\overset{\circ}{T}$ and $\overset{1}{T}$, respectively |
| $\overset{\circ}{T}(\equiv\overset{\circ}{T}_{11})$, $\overset{1}{T}(\equiv\overset{1}{T}_{11})$ | notations used in numerical illustrations to denote the amplitude in the mode |
| (1, 1) | of the temperatures $\overset{\circ}{T}(x^\alpha)$ and $\overset{1}{T}(x^\alpha)$, respectively |
| $T_u$, $T_b$ | temperature amplitudes in mode (1, 1) of the temperature distribution over the upper and bottom shell surfaces, respectively |
| $v_\alpha$, $v_3$ | tangential and transversal displacement quantities of the mid-surface of plate/shell |
| $\mathring{v}_3$ | initial geometric imperfection |
| $x^i$ | curvilinear system of normal coordinates |
| $\psi$, $\psi_1$ | Airy's potential function and particular solution of eqn (23), respectively |
| $\phi$, $F_\omega$ | functions associated with transverse shear |
| $\lambda_m, \mu_n, m\pi/l_1, n\pi/l_2\lambda_1, \lambda_2$ | stiffness of the supports along the edges $x_1 = 0$, $l_1$ and $x_2 = 0$, $l_2$, respectively, in the tangential directions, to the mid-surface normal to the edge. |
| $\lambda$, $\lambda'(\alpha, \alpha')$ | thermal expansion (compliance) coefficients in the tangential and transversal direction to the isotropy surface, respectively |
| $\delta_0(\equiv\mathring{w}_{11}/h)$, $\delta(\equiv w_{11}/h)$ | dimensionless amplitudes of the transverse deflection and of initial geometric imperfection, respectively |

| | |
|---|---|
| $\delta^i_j$ | Kronecker delta |
| $\Delta_1$ | end-shortening in the $x_1$-direction |
| $\omega^2$, $\bar{\omega}^2$ | fundamental frequency squared and its dimensionless counterpart, respectively |
| $(\cdot)_f$, $(\cdot)_c$ | quantities affiliated with face and core layers, respectively |
| $\sigma$ | mid-surface of the undeformed laminated structure |
| $\Lambda$, $\Pi$ | stretching and bending thermal stiffness quantities, respectively |
| $\tilde{\Lambda}$ | modified stretching thermal stiffness |
| $v$, $v'$ | Poisson's ratios tangential and transversal to the isotropy surface, respectively |
| $(\,)_{,i}$ | partial differentiation with respect to coordinates $x^i$ |
| $(\,)\|_i$, $(\,)\|_\alpha$ | covariant differentiation with respect to the metric tensor $g_{ij}$ and $a_{\alpha\beta}$, respectively. |
| $(\cdot)_{\langle r\rangle}$, $(\cdot)_{(r)}$ | affiliation of $(\cdot)$ to the $r$th layer and to the interlaminar surface defined by $x^3 = h_r$, respectively. |

## 1. Introduction

The static and dynamic behaviour of mechanically and thermally loaded flat and curved panels is a problem of considerable relevance in the design and development of supersonic/hypersonic vehicles, of future reusable space transportation, launch vehicles and of advanced propulsion systems. During their missions, the structure of flight vehicles have to withstand severe aerodynamic, aeroacoustic and thermomechanical loads. The temperatures involved are likely to range from the extreme lows of cryogenic fuels and radiation to space, to the highs associated with aerodynamic heating, heat from propulsion unit and radiation from the Sun. In spite of the increased flexibility which is likely to characterize the structure of next generations of advanced flight vehicles, they have to be able to fulfil a multitude of missions in complex environmental conditions and feature an expanded operational envelope. The same is valid with the reusable space vehicles, which, for evident reasons, require a prolongation of their operational life, without impairing upon the security of flight. A problem of evident importance towards the rational design of advanced supersonic/hypersonic flight vehicles lies in the possibility to accurately determine the load carrying capability of their structure. Moreover, a better understanding of conditions yielding an enhancement of the load carrying capacity, can dramatically contribute to the increase in performance of these flight vehicles. For curved panels such an investigation has a special significance. Indeed, in contrast to flat panels which experience a considerable amount of additional load-carrying capability in the postbuckling range, the curved panels exhibit a highly unstable postbuckling behavior, manifested by snap-through jumps toward a state of stable equilibrium. Such snapping jumps are manifested in both the static case (i.e. in the case e.g. of the temperature/compressive load vs transverse deflection response), and of the dynamic case (i.e. of eigenfrequency vs temperature/compressive load interaction). In addition, the load carrying capacity of curved panels is imperfection sensitive. It appears evident that reduction of the intensity of the snapping phenomenon and of the sensitivity to initial geometric imperfection, in general, and the accurate evaluation of the load carrying capacity, in particular, are of considerable importance toward a prolonged and exhaustive use of curved panels in the postbuckling range.

One of the modern trends in the construction of advanced flight vehicles capable of operating in a high temperature environment, consists of the ongoing incorporation in their structure of

advanced composite materials. However, as a result of this trend and for a reliable determination of their load carrying capacity, a careful assessment of the implications played by a number of non-classical effects is required. One of these is related with the transverse shear flexibility featured by advanced composites, and, in this connection, the problem of adequacy of Love–Kirchhoff shell model when dealing with thermomechanical load carrying capacity has to be addressed.

Another effect which was identified as the main cause of the large discrepancies between the experimental and theoretical predictions of buckling loads, and which can affect dramatically the load carrying capabilities of curved structures exposed to thermomechanical loading is the initial geometric imperfection.

The recent developments related with solid-propellant rocket motors, as well as the interest of specialists for developing further efficient thermal protection systems of space transportation vehicles have intensified the need for a better understanding of the non-linear response of geometrically perfect/imperfect shells continuously supported by elastic media and subjected to combined thermomechanical loadings. This issue will also be addressed in this paper.

Determination of frequency–temperature and frequency–load interactions in the pre/postbuckling ranges of curved panels featuring transverse shear flexibility, initial geometric imperfection, is of prime importance towards a reliable prediction of the aeroelastic behavior, thermoacoustic fatigue as well as of the dynamic response under time dependent external excitation of supersonic/hypersonic flight vehicle structures.

Another effect which becomes relevant in the context of multilayered shells composed of advanced composite materials is of a modeling nature. This effect is related with the non-fulfilment of the continuity requirement of transverse stresses at the layer interfaces. As was revealed in a number of recent papers (see e.g. Timarci and Soldatos, 1995; Xavier et al., 1995; Di Sciuva and Icardi, 1996; Librescu and Lin, 1996; Carrera, 1996, 1998; Carrera and Kroplin, 1997; Librescu et al., 1997), the violation of this requirement can result in unavoidable errors in the evaluation of the global response of laminated composite structures. These errors can even be exacerbated when the constituent materials exhibit large variations of transverse shear moduli from layer to layer. The assessment of the implications of the violation of this requirement, considered in conjunction with the other effects, previously mentioned, constitutes the basic goal of this paper. The implications induced by the non-fulfilment of the interlaminar shear traction continuity conditions upon the thermomechanical non-linear response will be analyzed by comparing the predictions based upon the shell/plate structural model developed in the papers by Librescu and Chang (1992, 1993), Librescu et al. (1993, 1995), Librescu and Lin (1997a, b) with their counterparts, obtained in the context of a theory fulfilling this requirement. Towards the goal of elucidating this problem, the basic kinetic equations associated with geometrically non-linear shell model fulfilling both the kinematic and static interlaminar continuity requirements will shortly be presented.

To the best of the authors' knowledge, geometrically non-linear theories of laminated shells fulfilling the interlaminar continuity conditions have been developed, in specialized contexts, in Librescu et al. (1997), Librescu and Schmidt (1991), Di Sciuva (1992), Schmidt and Librescu (1994), Pai and Nayfeh (1994), He (1995). For the sake of identification, in the forthcoming developments, the model fulfilling both interlaminar requirements is labeled as Model II, while the one violating the static interlaminar continuity requirement, as Model I.

In spite of the evident importance, studies devoted to this topic are extremely scarce, a fact which clearly emerges from the recent papers surveying the state-of-the-art of laminated shells (see

e.g. Noor and Burton, 1990, 1992; Reddy and Robbins, 1994; Librescu and Lin, 1996). To the best of the authors' knowledge, the available results addressing several of these issues restricted to linear response and static postbuckling of plates and shells subjected to compressive edge loads, have been presented by Librescu and Lin (1996) and Librescu et al. (1996), respectively. The goal of the paper is to supply additional information on this topic, by considering the static and dynamic non-linear response of laminated shell/plate structures when exposed to edge compression, lateral pressure and a temperature field, and by including additional effects not yet considered so far.

## 2. Preliminaries

Although the numerical illustrations will be applied to three-layer laminated shells and plates, for the sake of generality, the theory concerns the case of symmetric laminates constructed of $2m+1$ $(m = 1, 2, \ldots)$ laminae, the constituent material layers featuring monoclinic symmetry properties with respect to the global mid-surface of the structure. One assumes that the layers are in perfect bond, implying that no slip or debonding between two contiguous layers may occur. The employed notations follow, mainly, the ones used in Librescu and Chang (1992), Librescu et al. (1993, 1995) Librescu and Lin (1997a, b). Accordingly, the points of the 3-D shell space are referred to a set of curvilinear normal system of coordinates $x^i$, where $x^\alpha$ $(\alpha = 1, 2)$, denote the tangential coordinates, $x^3$ $(x^3 \leqslant |h/2|)$, being the normal coordinate to the reference surface $\sigma$ selected to coincide with the mid-surface of the mid-layer, while $h$ denotes the uniform thickness of the plate or shell.

The present study will be carried out in the context of the shallow shell theory (henceforth abbreviated as the SST).

Denoting by $Z(\equiv Z(x^\omega))$ the amount of deviation of the shell reference surface from its projection to a plan $P$, it is assumed that this quantity is small when compared with a maximum length of an edge of the shell, or with the minimum radius of curvature of $\sigma$. Postulating (see e.g. Green and Zerna, 1968) that

$$\max(\partial Z/\partial x^\omega) \ll 1 \tag{1}$$

it results that the metric tensors associated with the system of coordinates on $\sigma$ and with its projection on the plane $P$ are the same and, in addition, that the curvature tensor of the reference surface behaves as a constant in the differentiation operation. Consistent with the assumptions proper to the SST, we may appropriately consider

$$\mu^\alpha_\beta(\equiv \delta^\alpha_\beta - x^3 b^\alpha_\beta) \to \delta^\alpha_\beta \quad \text{and} \quad (\mu^{-1})^\alpha_\beta \to \delta^\alpha_\beta \tag{2a,b}$$

where $\mu^\alpha_\beta$ and its inverse $(\mu^{-1})^\alpha_\beta$ play the role of shifters in the space of normal coordinates (see Naghdi, 1963; Librescu, 1975). In eqns (2), $\delta^\alpha_\beta$ and $b^\alpha_\beta$ denote the Kronecker delta and the mixed curvature tensor, respectively. In addition, by virtue of the same assumptions we may obtain for the SST

$$\mu \equiv |\mu^\alpha_\beta| = 1 - 2x^3 H + K(x^3) \to 1 \tag{3}$$

where $H$ and $K$ denote the mean and Gaussian curvatures of $\sigma$, respectively. Moreover, by virtue of eqns (2), for the SST there is valid also

$$g^{\alpha\beta} = a^{\alpha\beta}; \quad g_{\alpha\beta} = a_{\alpha\beta} \tag{4}$$

where $g_{ij}(g^{ij})$ and a $a_{\alpha\beta}(a^{\alpha\beta})$ denote the covariant (contravariant) space and mid-surface metric components, respectively.

In order to reduce the 3-D elasticity problem to an equivalent 2-D one, the equations connecting the covariant derivatives of space tensors with their surface counterparts (identified by an overbar) are used. Several such relations restricted to the case of shallow surfaces are displayed next:

$$T_{\alpha\|\beta} = \bar{T}_{\alpha|\beta} - b_{\alpha\beta}\bar{T}_3; \quad T_{\alpha\|3} = \bar{T}_{\alpha,3}$$
$$T_{3\|\alpha} = \bar{T}_{3,\alpha} + b^{\nu}_{\alpha}\bar{T}_{\nu}; \quad \bar{T}_{3\|3} = \bar{T}_{3,3}$$
$$T^{\alpha\beta}_{\|\gamma} = \bar{T}^{\alpha\beta}_{|\gamma} - b^{\beta}_{\gamma}\bar{T}^{\alpha 3} - b^{\alpha}_{\gamma}\bar{T}^{3\beta}. \tag{5a–e}$$

These relationships (as well as the other ones not presented here) can be obtained by specializing, in the spirit of (2)–(4) for the SST case, the more general ones obtained for the theory of deep shells in Naghdi (1963) and Librescu (1975).

Here and in the following, partial differentiation is denoted by a comma $(\cdot)_{,i} \equiv \partial(\cdot)/\partial x_i$, while $(\,)\|_i$ and $(\,)|_\alpha$ stand for the covariant differentiations with respect to the space and surface metric, respectively, while the shifted components are identified by an upper bar. In the above relationships (as well as in the following developments), the usual summation convention for the repeated indices is implied, where Latin indices range from 1–3 while the Greek indices range from 1–2. In addition, a subscript or superscript in the brackets '$\langle\ \rangle$' attached to any quantity identifies its affiliation to the $k$-th layer. In spite of mathematical simplifications implied by the adoption of the shallow shell theory, the obtained results are rather general, being applicable to large categories of aeronautical structures. Moreover, this theory enables one to cast the geometrically non-linear equations in a form representing the generalized counterpart of the classical von Kármán–Mushtari–Marguerre large deflection shell theory. Such a form of the governing equations was proven to be of an exceptional usefulness in buckling and post-buckling studies.

## 3. Structural model

In order to develop the laminated shells theory within the Model II, the following steps are followed:

### 3.1. Transverse shear stress distribution

In the absence of shear tractions on the outer bounding surfaces $x^3 = \pm h/2$ of the shell, the following variation of transverse shear stresses across the thickness of each $k$-th layer is postulated (see Librescu and Lin, 1996; Librescu et al., 1997)

$$S^{\alpha 3}_{\langle k\rangle}(x^\lambda, x^3; t) = E^{\alpha 3\omega 3}_{\langle k\rangle} f(x^3) F_\omega(x^\lambda; t) + B^{\alpha}_{(k)}(x^\lambda; t). \tag{6}$$

A similar representation of transverse shear stresses proposed by Ambartsumian (1967) within the linear theory of laminated plates was further used in Librescu and Reddy (1986).

In eqn (6), $f(x^3)$ is the function characterizing the variation of $S^{\alpha 3}$ across the shell thickness,

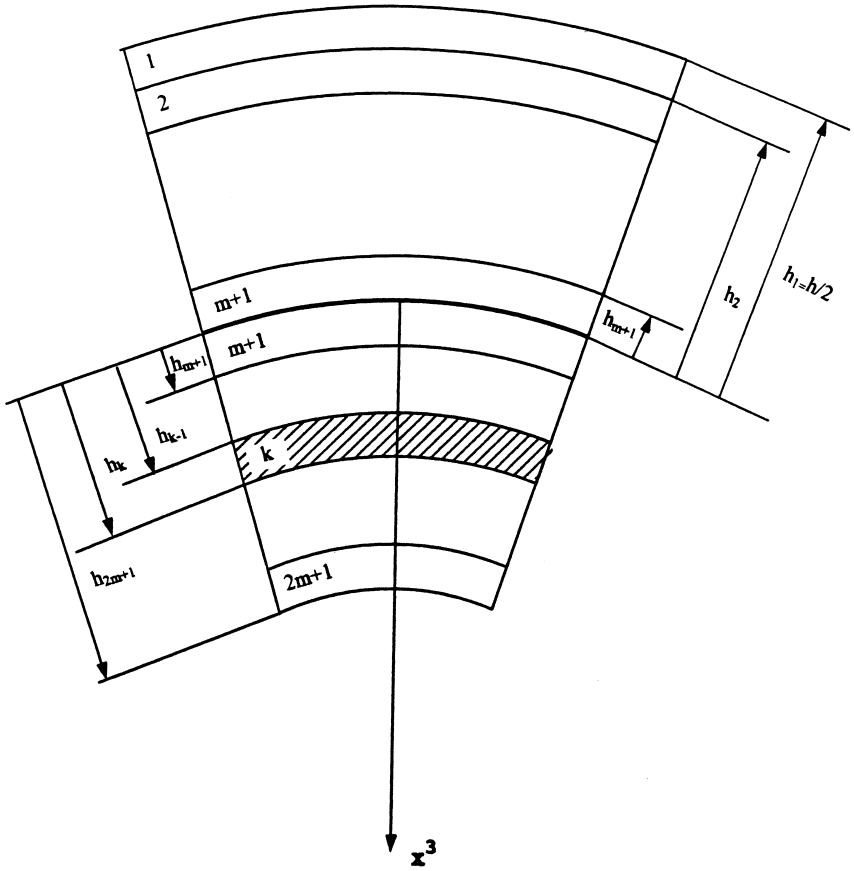


Fig. 1. Geometry of the cross-section of a symmetrically laminated shell.

while $t$ is the time variable. For the present case, $f$ is represented as an even function in the thickness coordinate in the sense of $f(x^3) = f(-x^3)$, and in order to fulfil the free traction condition on $x^3 \pm h/2$, one assumes, in addition (see Fig. 1)

$$f(h_1) = f(h_{2m+1}) = 0, \tag{7}$$

where $h_1$ and $h_{2m+1}$ define the location of the upper and bottom faces of the laminate, respectively, measured from the shell mid-surface. In addition, $F_\omega(\equiv F_\omega(x^\lambda; t))$, are yet unknown functions determining the shape of variation of $S^{\alpha 3}$ in the surfaces parallel to the mid-surface, while $B^\alpha_{(k)}(\equiv B^\alpha_{(k)}(x^\omega; t))$ are functions to be determined upon fulfilling the continuity requirement for interlaminar shear stresses

$$S^{\alpha 3}_{\langle k\rangle}|_{x^3=h_k} = S^{\alpha 3}_{\langle k-1\rangle}|_{x^3=h_k}. \tag{8}$$

Following further the procedure outlined in Librescu and Lin (1996) and Librescu et al. (1997), with the help of eqns (8) the expression of transverse shear stresses, eqn (6) modifies as

$$S^{\alpha 3}_{\langle k\rangle}(x^\lambda, x^3; t) = [E^{\alpha 3\omega 3}_{\langle k\rangle} f(x^3) + A^{\alpha 3\omega 3}_{(k)}]F_\omega(x^\lambda; t) \tag{9a}$$

where

$$B^{\alpha}_{(k)}(x^\lambda; t) = A^{\alpha 3\omega 3}_{(k)} F_\omega(x^\lambda; t). \tag{9b}$$

In eqns (8) and (9) $S^{\alpha 3}$ denote the transverse shear components of the second Piola–Kirchhoff stress tensor $S^{ij}$, while

$$A^{\alpha 3\omega 3}_{(k)} = -\sum_{r=2}^{k} f(h_r)[E^{\alpha 3\omega 3}_{\langle r\rangle} - E^{\alpha 3\omega 3}_{\langle r-1\rangle}]. \tag{10a}$$

Upon imposing also the condition $[x^3 S^{\alpha 3}]^{h/2}_{-h/2} = 0$, and having in view the symmetry of the construction which implies that $E^{\alpha 3\omega 3}_{\langle r\rangle} = E^{\alpha 3\omega 3}_{\langle 2m+2-r\rangle}$, one also obtains

$$A^{\alpha 3\omega 3}_{(r)} = A^{\alpha 3\omega 3}_{(2m+2-r)} \begin{cases} \text{for } r = 1 \\ = 0 \text{ for } r = 1 \end{cases}. \tag{10b}$$

As can easily be inferred from eqns (9) and (10), in case of mild variations of transverse shear moduli, implying $E^{\alpha 3\omega 3}_{\langle i\rangle} \approx E^{\alpha 3\omega 3}_{\langle i-1\rangle}$ and hence $A^{\alpha 3\omega 3}_{(i)} \to 0$, fulfilment of the interlaminar shear traction continuity requirement turns out to be quite a redundant matter. As a result, fulfilment of this condition has to be enforced whenever the materials of the laminae exhibit significant jumps in transverse shear moduli from layer to layer. In the previous equations, the subscript $r$ in the brackets ( ) attached to any quantities indicate their belonging to the interlamina surface defined by $x^3 = h_r$.

### 3.2. Tangential displacements in the thickness direction

Assuming that the structure features a stress-free small initial geometric imperfection $\mathring{V}_3(x^\omega, x^3; t)(\equiv \mathring{v}_3(x^\omega; t))$, considered to be positive when it is towards the downward direction and adopting the concept of small strains and moderately small rotations (Librescu, 1987), the 3-D strain–displacement relationship in Lagrangian description is:

$$2e_{ij} = V_{i\|j} + V_{j\|i} + V_{3\|i}V_{3\|j} + V_{3\|i}\mathring{V}_{3\|j} + \mathring{V}_{3\|i}V_{3\|j}, \tag{11}$$

where $V_i(\equiv V_i(x^\omega, x^3; t))$ denote the 3-D displacement components.

Postulating that

$$V_3(x^\omega, x^3; t) = v_3(x^\omega; t), \tag{12}$$

from eqn (11) one can extract the 3-D expression of transverse shear strains expressed in terms of displacement components as

$$2e^{\langle k\rangle}_{\lambda 3} = V^{\langle k\rangle}_{\lambda\|3} + V^{\langle k\rangle}_{3\|\lambda}. \tag{13}$$

Employment in eqn (13) of the relationships connecting covariant derivatives of space and surface tensors specialized for shallow shell theory, eqns (5) used in conjunction with the constitutive equations for $e^{\langle k\rangle}_{\lambda 3}$

$$e_{\lambda 3}^{\langle k\rangle} = 2F_{\lambda 3\mu 3}^{\langle k\rangle} S_{\langle k\rangle}^{\mu 3}, \tag{14}$$

as well as with eqn (9), yields

$$V_{\lambda,3}^{\langle k\rangle} = 4F_{\lambda 3\mu 3}^{\langle k\rangle}[E_{\langle k\rangle}^{\mu 3\gamma 3} f(x^3) + A_{(k)}^{\mu 3\gamma 3}]F_\gamma - v_{3,\lambda} - b_\lambda^\rho V_\rho^{\langle k\rangle}. \tag{15}$$

In eqn (15), $F_{\lambda 3\mu 3}^{\langle k\rangle}$ stands for the compliance components corresponding to $E_{\langle k\rangle}^{\lambda 3\omega 3}$, related by $E_{\langle k\rangle}^{\lambda 3\omega 3} F_{\lambda 3\beta 3}^{\langle k\rangle} = \delta_\beta^\omega/4$ (see Librescu, 1975).

Integration of eqn (15) with respect to $x^3$ in the interval $[0, x^3)$ and employment of eqn (12) yields:

$$V_\lambda^{\langle k\rangle}(x^\omega, x^3; t) = \hat{V}_\lambda^{\langle k\rangle} - x^3 v_{3,\lambda} + F_\gamma[\delta_\gamma^\gamma J_0(x^3) + 4x^3 F_{\lambda 3\mu 3}^{\langle k\rangle} A_{(k)}^{\mu 3\gamma 3}]. \tag{16}$$

In eqn (16)

$$J_0(x^3) = \int_0^{x^3} f(x^3)\,\mathrm{d}x^3, \tag{17}$$

where $\hat{V}_\lambda^{\langle k\rangle} (\equiv \hat{V}_\lambda^{\langle k\rangle}(x^\omega; t))$ are arbitrary functions of integration. Upon fulfilling the kinematic interlaminar continuity conditions

$$V_\lambda^{\langle k+1\rangle}|_{x^3 = h_k} = V_\lambda^{\langle k\rangle}|_{x^3 = h_k} \tag{18}$$

and having in view that

$${}^{\langle m+1\rangle}V_\lambda|_{x^3 = 0^+} = {}^{\langle m+1\rangle}V_\lambda|_{x^3 = 0^-} \equiv v_\lambda(x^\omega; t) \tag{19}$$

represent the displacement components of the mid-surface of the laminate mid-layer, one obtains

$${}^{\langle k\rangle}\hat{V}_\lambda(x^\omega; t) = v_\lambda - 4{}^{(k)}\Omega_\lambda^\gamma F_\gamma \operatorname{sgn} x^3, \quad (k = 1, 2, \ldots, m) \tag{20}$$

where $\operatorname{sgn} x^3$ ($=1$ for $x^3 > 0$; $= 0$ for $x^3 = 0$ and $= -1$ for $x^3 < 0$), denotes the signum distribution, while

$${}^{(k)}\Omega_\lambda^\gamma = \sum_{r=2}^{k} h_{r-1}[F_{\lambda 3\mu 3}^{\langle r\rangle} A_{(r)}^{\mu 3\gamma 3} - F_{\lambda 3\mu 3}^{\langle r-1\rangle} A_{(r-1)}^{\mu 3\gamma 3}]. \tag{21}$$

Upon invoking the symmetry of the laminate with respect to its mid-surface, it results ${}^{(k)}\Omega_\lambda^\gamma = {}^{(2m+2-k)}\Omega_\lambda^\gamma$ and ${}^{(m+1)}\Omega_\lambda^\gamma = 0$. Equations (16) considered in conjunction with eqn (20) reveals that in the context of this theory, the tangential displacement components assume a non-linear variation in the thickness direction, its character being decided by the character of the variation of $J_0(x^3)$ in the thickness direction.

### 3.3. Tangential strain representation

Upon invoking in eqn (11) the relationships between covariant derivatives of 3-D and surface tensors, in conjunction with eqns (16) and (20), one obtains

$$\begin{aligned} {}^{\langle k\rangle}e_{\alpha\beta} = {} & -x^3 v_{3|\alpha\beta} + \tfrac{1}{2}J_0(x^3)(F_{\alpha|\beta} + F_{\beta|\alpha}) + 2x^3(F_{\alpha 3\mu 3}^{\langle k\rangle} A_{(k)}^{\mu 3\gamma 3} F_{\gamma|\beta} + F_{\beta 3\mu 3}^{\langle k\rangle} A_{(k)}^{\mu 3\gamma 3} F_{\gamma|\alpha}) \\ & - 2({}^{(k)}\Omega_\alpha^\gamma F_{\gamma|\beta} + {}^{(k)}\Omega_\beta^\gamma F_{\gamma|\alpha}) \operatorname{sgn} x^3 + \tfrac{1}{2}(v_{\alpha|\beta} + v_{\beta|\alpha} - 2b_{\alpha\beta}v_3) + v_{3,\alpha}v_{3,\beta} + v_{3,\beta}\mathring{v}_{3,\alpha} + \mathring{v}_{3,\alpha}v_{3,\beta} \end{aligned} \tag{22}$$

Equation (22) reveals that the tangential strain components feature a variation through the shell thickness, similar to that of tangential displacement components, eqn (16).

### 3.4. Constitutive equations

As is well known (see e.g. Malvern, 1969), the 3-D elasticity theory implying small strains but large displacement gradients can be described by linear constitutive equations relating second Piola–Kirchhoff stress tensor $S^{ij}$ with Lagrangian strain tensor $e_{ij}$.

As a result, postulating as usual that transverse normal stress component $S^{33}$ in constitutive equations is negligibly small compared with the other stresses, and proceeding to the elimination of the transverse normal strain $e_{33}$, the 3-D constitutive equations pertinent to a material featuring monoclinic symmetry properties become

$$S^{\alpha\beta} = \tilde{E}^{\alpha\beta\omega\rho} e_{\omega\rho} + \tilde{\lambda}^{\alpha\beta} T; \quad S^{\alpha 3} = 2E^{\alpha 3\omega 3} e_{\omega 3}, \tag{23a,b}$$

where

$$\tilde{E}^{\alpha\beta\omega\rho} = E^{\alpha\beta\omega\rho} - \frac{E^{\alpha\beta 33} E^{33\omega\rho}}{E^{3333}}; \quad \tilde{\lambda}^{\alpha\beta} = \lambda^{\alpha\beta} - \frac{E^{\alpha\beta 33}}{E^{3333}} \lambda^{33}. \tag{24}$$

In these equations $E^{ijmn}$ and $\lambda^{ij}$ denote the tensors of elastic moduli and of the thermal compliance coefficients, respectively, assumed to be temperature independent, while $T(\equiv T(x^{\omega}, x^3))$ denotes the temperature rise from a stress-free reference temperature $T_r$.

Employment, in conjunction with eqns (22) and (23) of expressions defining within the SST the (membrane $L^{\alpha\beta}$ and transverse shear $Q^{\alpha\beta}$) stress resultants, and stress couples $M^{\alpha\beta}$, namely

$$(N^{\alpha\beta}, M^{\alpha\beta}) = 2\int_0^{h_{m+1}} S^{\alpha\beta}_{\langle m+1\rangle}(1, x^3)\,\mathrm{d}x^3 + 2\sum_{r=1}^{m}\int_{h_{r-1}}^{h_r} S^{\alpha\beta}_{\langle r-1\rangle}(1, x^3)\,\mathrm{d}x^3, \tag{25a}$$

$$Q^{\alpha 3} = 2\int_0^{h_{m+1}} S^{\alpha 3}_{\langle m+1\rangle}\,\mathrm{d}x^3 + 2\sum_{r=1}^{m}\int_{h_{r-1}}^{h_r} S^{\alpha 3}_{\langle r-1\rangle}\,\mathrm{d}x^3, \tag{25b}$$

yields the constitutive equations of the shell theory:

$$N^{\alpha\beta} = \mathscr{F}^{\alpha\beta\omega\rho}\varepsilon_{\omega\rho} + \Lambda^{\alpha\beta}\overset{\circ}{T} \tag{26a}$$

$$Q^{\alpha 3} = \mathscr{K}^{\alpha 3\omega 3} F_{\omega} \tag{26b}$$

$$M^{\alpha\beta} = -\mathscr{D}^{\alpha\beta\omega\rho} v_{3,\omega\rho} + (\mathscr{T}^{\alpha\beta\omega\rho} + \mathscr{L}^{\alpha\beta\omega\rho} - \mathscr{S}^{\alpha\beta\omega\rho})(F_{\omega|\rho} + F_{\rho|\omega}) + \Pi^{\alpha\beta}\overset{1}{T}. \tag{26c}$$

Herein $\varepsilon_{\alpha\beta}$ denotes the membrane strain tensor defined as

$$\varepsilon_{\alpha\beta} = \tfrac{1}{2}(v_{\alpha,\beta} + v_{\beta,\alpha} - 2b_{\alpha\beta}v_3) + v_{3,\alpha}v_{3,\beta} + v_{3,\alpha}\overset{\circ}{v}_{3,\beta} + \overset{\circ}{v}_{3,\alpha}v_{3,\beta} \tag{27}$$

and $\overset{0}{T}(\equiv \overset{0}{T}(x^{\omega}))$ and $\overset{1}{T}(\equiv \overset{1}{T}(x^{\omega}))$ define the membrane and thicknesswise temperature distributions, respectively, in whose terms the 3-D temperature field is expressed as

$$T(x^{\omega}, x^3) = \overset{\circ}{T}(x^{\omega}) + x^3\overset{1}{T}(x^{\omega}). \tag{28}$$

Herein, $\overset{\circ}{T} = (T_u + T_b)/2$ and $\overset{1}{T} = (T_b - T_u)/h$, where $T_u = T(x^\omega, -h/2)$ and $T_b = T(x^\omega, h/2)$. In addition, $\mathscr{F}^{\alpha\beta\omega\rho}, \ldots, \mathscr{L}^{\alpha\beta\omega\rho}$ and $\Lambda^{\alpha\beta}$, $\Pi^{\alpha\beta}$ denote the elastic and thermal stiffness quantities, respectively, whose expressions are displayed in Appendix 1.

The previously displayed kinematic equations contain five unknown functions, namely three kinematic quantities, $v_\alpha(x^\omega; t)$, $v_3(x^\omega; t)$ and the two static ones, $F_\alpha(x^\omega; t)$. As a result, in order to generate the governing equations expressed in terms of these functions, five 2-D equations of motion are needed.

These are obtained by taking the various moments of the equations of equilibrium of the 3-D non-linear elasticity theory

$$[S^{jr}(\delta^i_r + V^i\|_r + \overset{\circ}{V}{}^i\|_r)]\|_j = \rho_0 \ddot{V}^i. \tag{29}$$

Use of the approximation proper to the shallow shell theory, followed by the consideration in eqns (29) of moments of order zero and one of the equations corresponding to $i = 1, 2$ and of the moment of order zero of the equations corresponding to $i = 3$, with the help of eqns (5) and (12), by discarding the tangential and rotary inertia terms, one obtains the two-dimensional equations of motion as:

$$N^{\alpha\beta}|_\beta = 0; \quad M^{\alpha\beta}|_\beta - Q^{\alpha 3} = 0, \tag{30a,b}$$

$$b_{\rho\alpha}N^{\alpha\rho} + N^{\alpha\rho}(v_{3,\beta} + \overset{\circ}{v}_{3,\beta})|_\alpha + Q^{\alpha 3}|_\alpha + p_3 = m_0\ddot{v}_3 \tag{30c}$$

where $p_3(\equiv p_3(x^\omega))$ denotes the distributed transversal load, $m_0(\equiv 2[\rho_{\langle m+1\rangle}h_{m+1} + \Sigma_{r=1}^m \rho_{\langle m\rangle}(h_r - h_{r-1}])$ stands for the reduced mass, while the superposed dots denote time derivatives.

Upon expressing $N^{\alpha\beta}$ in terms of the Airy's potential function $\psi(\equiv\psi(x^\omega; t)$ as

$$N^{\alpha\beta} = c^{\alpha\omega}c^{\beta\rho}\psi\,|_{\omega\rho}, \tag{31}$$

where $c^{\alpha\beta}$ denotes the 2-D permutation symbol, eqn (30a) is identically satisfied. In this case, the compatibility equation associated with the membrane strains $\varepsilon_{\alpha\beta}$ has to be included as a primary equation of the non-linear boundary-value problem. It is

$$c^{\alpha\pi}c^{\beta\lambda}[\varepsilon_{\alpha\beta|\pi\lambda} + \tfrac{1}{2}v_{3|\alpha\rho}v_{3|\lambda\pi} + \tfrac{1}{2}\overset{\circ}{v}_{3|\pi\lambda}v_{3|\alpha\beta} + \tfrac{1}{2}v_{3|\pi\lambda}\overset{\circ}{v}_{3|\alpha\beta} + b_{\alpha\beta}v_{3|\pi\lambda}] = 0. \tag{32}$$

## 4. Governing system

For the problem to be studied in the present paper, a most convenient representation of the governing equations is in the form constituting the extended counterpart of the classical von Kármán–Mushtari–Marguerre large deflection shell theory. To this end, and in order to simplify the problem without impairing upon the generality of the conclusions, a special type of anisotropy of the constituent materials will be considered. The anisotropy is of a transversely-isotropic type, where the surface of isotropy is parallel at each point to the mid-surface $\sigma$.

Due to the distinct thermomechanical properties in the transverse and tangential directions to the shell mid-surface, these materials (known as pyrolytic–graphite materials), are good candidates

for being used in the design of the thermal protection of aerospace vehicles and engine nozzles (see e.g. Woods, 1976).

For such a material, the expressions of the thermo-elastic moduli are (see Librescu, 1975)

$$\tilde{E}^{\alpha\beta\omega\rho} = \frac{E}{1+v}\left[\frac{1}{2}(a^{\alpha\omega}a^{\beta\rho}+a^{\omega\beta}a^{\alpha\rho})+\frac{v}{1-v}a^{\omega\rho}a^{\alpha\beta}\right],$$

$$E^{\alpha 3\omega 3} = G' a^{\alpha\omega}, \quad \tilde{\lambda}^{\alpha\beta} = \tilde{\lambda}a^{\alpha\beta} \equiv \lambda \mathscr{A} a^{\alpha\beta} \tag{33a–c}$$

where

$$\mathscr{A} = \begin{cases} 1-\dfrac{Ev'}{E'(1-v)}\dfrac{\lambda'}{\lambda} & \text{for transversely-isotropic materials} \\ \dfrac{1-2v}{1-v} & \text{for isotropic materials.} \end{cases} \tag{34}$$

$E(E')$, $v(v')$, $\lambda(\lambda')$ are the Young's modulus, Poisson's ratio and thermal compliance coefficient in the plane of isotropy (transversal to the plane of isotropy), and $G'$ is the transverse shear modulus.

As usual, the ratio $E/G'$ constitutes a measure of the transverse shear flexibility of the material. Adoption of Love–Kirchhoff shell model requires that $E/G' \to 0$, this reverting to the conclusion that in the context of the classical shell model, the constituent materials feature an infinite stiffness in transverse shear (i.e. that $G' \to \infty$).

As a first step towards obtaining the governing equations, the expression of $\varepsilon_{\alpha\beta}$ obtained from eqn (26a) under the form

$$\varepsilon_{\pi\sigma} = \mathscr{P}_{\alpha\beta\pi\sigma}\mathscr{L}^{\alpha\beta} - \tilde{\Lambda}_{\pi\sigma}\overset{\circ}{T} \tag{35}$$

used in conjunction with eqn (31), is replaced in eqn (36). Here $\mathscr{P}_{\alpha\beta\pi\rho}$ is the inverse of $\mathscr{F}^{\alpha\beta\omega\pi}$ in the sense of

$$\mathscr{P}_{\alpha\beta\lambda\sigma}\mathscr{F}^{\alpha\beta\omega\rho} = \tfrac{1}{2}(\delta^{\omega}_{\lambda}\delta^{\rho}_{\sigma}+\delta^{\rho}_{\lambda}\delta^{\omega}_{\sigma}) \tag{36}$$

and

$$\tilde{\Lambda}_{\pi\sigma} = \mathscr{P}_{\alpha\beta\pi\sigma}\Lambda^{\alpha\beta}. \tag{37}$$

In such a way, for the considered type of material anisotropy, one of the governing equations expressed in terms of $\psi$ and $v_3$ is obtained and is given by

$$(\tilde{b}+\tilde{c})\psi|^{\lambda\pi}_{\lambda\pi}+\tfrac{1}{2}(v_3|^{\rho}_{\rho}v_3|^{\lambda}_{\lambda}-v_3|^{\lambda}_{\rho}v_3|\rho\lambda)+(\overset{\circ}{v}_3|^{\pi}_{\pi}v_3|^{\alpha}_{\alpha}-\overset{\circ}{v}_3|^{\pi}_{\alpha}v_3|^{\alpha}_{\pi})+(2Hv_3|^{\pi}_{\pi}-b^{\beta}_{\lambda}v_3|^{\lambda}_{\beta})+\tilde{\Lambda}\overset{\circ}{T}|^{\alpha}_{\alpha} = 0 \tag{38}$$

where $\tilde{b}$, $\tilde{c}$ and $\tilde{\Lambda}$ are defined in Appendix 2.

At this point, the equations of motion, (30b,c) in conjunction with the constitutive eqns (26b,c) for the case of transversely-isotropic materials are used. As a result, one obtains

$$-\mathscr{D}v_3|^{\alpha\beta}_{\beta}+(\mathscr{T}_1+\mathscr{L}_1+\mathscr{S}_1)F^{\alpha}|^{\beta}_{\beta}+(\mathscr{T}_2+\mathscr{L}_2+\mathscr{S}_2)F^{\beta}|^{\alpha}_{\beta}-\mathscr{K}F^{\alpha}+\overset{1}{\Pi}T|^{\alpha} = 0, \tag{39a}$$

$$\mathscr{K}F^{\alpha}|_{\alpha}+b_{\alpha\rho}N^{\alpha\rho}+N^{\alpha\rho}(v_{3,\beta}+\mathring{v}_{3,\beta})|_{\alpha}+p_3=m_0\ddot{v}_3. \tag{39b}$$

Following the procedure developed in a number of previous works e.g. in Librescu and Chang (1992, 1993), Librescu and Lin (1996) and Librescu (1975), upon expressing $F^{\alpha}(x^{\omega};t)$ in terms of a new potential $\phi(x^{\omega};t)$ as

$$\mathscr{K}F^{\alpha}=-c^{\omega\alpha}\phi|_{\omega}-\mathscr{D}v_3|^{\alpha\beta}_{\beta}-\frac{1}{\mathscr{K}}(\mathscr{T}+\mathscr{L}+\mathscr{S})\{p_3|^{\alpha}-m_0\ddot{v}_3|^{\alpha}$$
$$+[N^{\omega\rho}(v_{3|\omega\rho}+\mathring{v}_{3|\omega\rho})]|^{\alpha}+b_{\rho\omega}N^{\omega\rho}|^{\alpha}\}+\overset{1}{\Pi}T|^{\alpha} \tag{40}$$

and using the representation for $N^{\alpha\beta}$ given by eqn (31), two governing equations are obtained. These are

$$\mathscr{D}v_3|^{\alpha\beta}_{\alpha\beta}-c^{\omega\alpha}c^{\rho\beta}\left\{b_{\rho\omega}\psi|_{\alpha\beta}+(v_{3|\omega\rho}+\mathring{v}_{3|\omega\rho})\psi_{|\alpha\beta}-\frac{\mathscr{T}+\mathscr{L}+\mathscr{S}}{\mathscr{K}}(b_{\rho\omega}\psi_{|\alpha\beta}+\psi_{|\alpha\beta}(v_{3|\rho\omega}+\mathring{v}_{3|\rho\omega}))|^{\sigma}_{\sigma}\right\}$$
$$-\left(p_3-\frac{\mathscr{T}+\mathscr{L}+\mathscr{S}}{\mathscr{K}}p_3|^{\alpha}_{\alpha}\right)+m_0\left(\ddot{v}_3-\frac{\mathscr{T}+\mathscr{L}+\mathscr{S}}{\mathscr{K}}\ddot{v}_3|^{\alpha}_{\alpha}\right)-\overset{1}{\Pi}T|^{\alpha}_{\alpha}=0 \tag{41a}$$

and

$$\phi-\frac{\mathscr{T}_1+\mathscr{L}_1+\mathscr{S}_1}{\mathscr{K}}\phi|^{\alpha}_{\alpha}=0. \tag{41b}$$

In these equations $\mathscr{D}$, $\mathscr{T}(\equiv\mathscr{T}_1+\mathscr{T}_2)$, $\mathscr{L}(\equiv\mathscr{L}_1+\mathscr{L}_2)$, $\mathscr{S}(\equiv\mathscr{S}_1+\mathscr{S}_2)$ and $\mathscr{K}$ are stiffness quantities whose expressions are recorded in Appendix 2. In addition $(\cdot)|^{\alpha}_{\alpha}$ and $(\cdot)|^{\alpha\beta}_{\alpha\beta}$ denote the 2-D Laplace and biharmonic operators, respectively; $2H(\equiv b_{\alpha\beta}a^{\alpha\beta}=(1/R_1+1/R_2))$ denotes the mean curvature of $\sigma$, where $R_{\alpha}$ denote the principle radii of curvature of $\sigma$.

Equations (38) and (41a,b) represent the governing system of partial differential equations pertinent to the geometrically non linear theory of shallow shells, symmetrically laminated of transversally isotropic material layers. In these equations the higher-order effects, the temperature, the dynamic and the initial geometric imperfection effects have been included.

The previously obtained governing equation system constitutes the generalized counterpart of that previously obtained in different contexts (see Librescu and Chang, 1992, 1993; Librescu et al., 1993, 1995; Librescu and Lin, 1996). It should be underlined that in this form, the governing system is similar to the one obtained in the previously mentioned papers where only the kinematic continuity requirement was fulfilled. The difference occurs in the expressions of stiffness quantities only. The correspondence between the two group of stiffness quantities is:

$$C\leftrightarrow\mathscr{T}_1+\mathscr{L}_1+\mathscr{S}_1;\quad S\leftrightarrow\mathscr{K}\quad B\leftrightarrow\mathscr{T}_2+\mathscr{L}_2+\mathscr{S}_2. \tag{42a–c}$$

The correspondence sign '↔' is intended to suggest that the group of governing eqns (38) and (41a,b) pass into its counterpart, obtained without fulfilling the transverse shear stress continuity requirement, and vice versa, when the change of stiffness quantities indicated in eqns (42) is carried out.

As concerns the stiffness quantities not involved in these correspondence, i.e. $\mathscr{D}$, $\tilde{b}$, $\tilde{c}$, $\Pi$, $\Lambda$, $\tilde{\Lambda}$, these remain unchanged in the two structural models. The expressions of the stiffness quantities

$C$, $B$ and $S$ are displayed in Appendix 3. The classical counterpart of the previously obtained governing system, is obtained by letting $\mathscr{K} \to \infty$.

In the case of a single layered shell, in the stiffness quantities (see Appendices 1 and 2), the specializations

$$h_{m+1} \to h/2, \quad \sum_{r=1}(\cdot) \to 0 \tag{43a,b}$$

have to be carried out. In the case involving eqns (43), when $f(x^3)$ is considered to be $f(x^3) = (x^3)^2 - h^2/4$, it can readily be verified that the governing equations associated with the two structural models collapse into a unique one, coinciding with the one derived by Librescu (1975). This expression will be also considered in the numerical illustrations displayed in this paper. For other representations of $f(x^3)$ see Ambartsumian (1967).

In the case of the shell supported on the inner surface by a Winkler non-linear elastic foundation, $p_3$ in eqn (41a) should be modified as (see also Librescu and Lin, 1997)

$$p_3(x^\omega) \to \hat{p}_3 - (\bar{K}_1 v_3 + \bar{K}_3 (v_3)^3), \tag{44}$$

where $\hat{p}_3 (\equiv \hat{p}_3(x^\omega))$ denotes the distributed lateral pressure acting on the outer face of the shell, while $\bar{K}_1$ and $\bar{K}_3$ are the linear and cubic Winkler foundation moduli, respectively.

It should be mentioned that the linear eqn (41b), of a Helmholtz-type, defines the boundary-layer effect. Its solution is characterized by a rapid decay when proceeding from the edges towards the interior of the shell. Although uncoupled with the remaining governing equations, the unknown function $\phi$ remains coupled with the other two functions, $\psi$ and $v_3$ in the equation is expressing the boundary conditions, in number of five at each edge.

As was shown previously (e.g. see Librescu and Stein, 1991; Librescu and Chang, 1992), for simply supported boundaries, the function $\phi$ can be rendered decoupled in the boundary condition, and as a result, the boundary layer equation (41b) in conjunction with the associated boundary conditions admits the trivial solution $\phi \equiv 0$. In such a case eqn (41b) can exactly be discarded and as a result, the order of governing equations reduces from ten to eight, yielding a reduction of the number of boundary conditions from five to four.

## 5. Non-linear response of flat and doubly curved shallow panels with rectangular planform

The non-linear response of doubly curved simply-supported panels of rectangular planform on the plane $P$ will be analyzed. The points of $\sigma$ are referred to a Cartesian orthogonal system of coordinates $x_\omega$ assumed to be parallel to the panel edges. We consider that the panel is subjected to: (i) a system of uniform in-plane biaxial compressive edge loads $\mathscr{N}_{11}$ and $\mathscr{N}_{22}$ defined by $L_R (\equiv \mathscr{N}_{22}/\mathscr{N}_{11})$, $L_R \gtrless 0$, depending on whether $\mathscr{N}_{22} \gtrless 0$, where the positive sign of the normal edge loads corresponds to compression; (ii) the uniaxial compressive load $\mathscr{N}_{11}$; (iii) a lateral pressure $\hat{p}_3(x_\omega)$; (iv) a temperature field; and (v) combinations of thermal and mechanical loading systems.

Depending upon the in-plane behavior in the direction normal to the edges, three cases, will be considered:

Case (A): The edges are simply supported and freely moveable in the direction normal to the unloaded edges in the plane tangent to the surface at the panel edges, and

Case (B): The edges are simply supported. Uniaxial edge loads are acting in the direction of the $x_1$-coordinate. The edges $x_1 = 0,\ l_1$ are considered freely moveable, the in-plane motion of the remaining two unloaded edges in direction normal to the edges being prevented. In the present case edges $x_2 = 0,\ l_2$ are referred to as immoveable.

In the case of the panel loaded in the direction of the $x_1$-coordinate only, the remaining edges being unloaded and immoveable, the condition for the immoveable edges $x_2 = 0,\ l_2$ may be expressed in an average sense as (see, e.g. Librescu et al., 1995; Librescu, 1975),

$$\int_0^{l_1}\int_0^{l_2} v_{2,2}\,\mathrm{d}x_1\,\mathrm{d}x_2 = 0, \tag{45}$$

where $v_2(\equiv b_2(x_1, x_2, t)$ denotes the tangential displacement parallel to the $x_2$-coordinate. This equation considered in conjunction with eqns (27), (35), (31), (47) and (46) yields the fictitious edge load $\mathscr{N}_{22}$ for which the edges $x_2 = 0,\ l_2$ remain immoveable.

Corresponding to the immoveable edges $x_n = \text{const}$ $(n = 1, 2)$, the boundary conditions are:

$$v_3 = N_{nt} = M_{nn} = F_t = 0, \quad N_{nn} = -\mathscr{N}_{nn}, \tag{46a}$$

whereas the ones corresponding to the moveable edges, $x_n = \text{const}$, these are:

$$v_3 = u_n = N_{nt} = M_{nn} = F_t = 0. \tag{46b}$$

Herein $n$ and $t$ designate the normal and tangential directions to the boundary, implying that $n = 1$ when $t = 2$, and vice versa, $n = 2$ when $t = 1$.

Case (C): In addition to the previously mentioned tangential edge restraint conditions, the case of partially moveable opposite unloaded edges $x_\alpha = 0,\ l_\alpha$ is considered. For this case, following, Librescu et al. (1995) and Librescu (1975), a measure of the partial movability of edges $x_\alpha = 0,\ l_\alpha$ $(x = 1, 2)$ in terms of the edge stiffness parameter $\lambda_\alpha$ is defined. As was shown in the above indicated references, moveable and immoveable edges $x_\alpha = 0, l_\alpha$ correspond to $\lambda_\alpha = 0$ and $\lambda_\alpha = 1$, respectively. Partially moveable edges at $x_\alpha = 0,\ l_\alpha$ are defined by $0 < \lambda_\alpha < 1$. As in the case of immoveable edges, also in this case, for a specific value of $\lambda_\alpha$, the necessary fictitious edge load $\mathscr{N}_{\alpha\alpha}$ rendering the edges $x_\alpha = 0,\ l_\alpha$ partially moveable has to be determined.

Considerations related with identical fulfilment of the out-of-plane boundary conditions and implementation of initial geometric imperfections yielding the most critical postbuckling behavior (see e.g. Seide, 1974; Simitses, 1986; Amazigo et al., 1970), suggest the following representations:

$$\begin{Bmatrix} v_3(x_1, x_2; t) \\ \mathring{v}_3(x_1, x_2) \end{Bmatrix} = \begin{Bmatrix} w_{mn}(t) \\ \mathring{w}_{mn} \end{Bmatrix} \sin\lambda_m x_1 \sin\mu_n x_2, \tag{47a}$$

$$\begin{Bmatrix} \overset{\circ}{T}(x_1, x_2) \\ \overset{1}{T}(x_1, x_2) \\ \hat{p}_3(x_1, x_2) \end{Bmatrix} = \begin{Bmatrix} \overset{\circ}{T}_{mn} \\ \overset{1}{T}_{mn} \\ p_{mn} \end{Bmatrix} \sin\lambda_m x_1 \sin\mu_n x_2, \tag{47b}$$

where $\lambda_m = m\pi/l_1;\ \mu_n \equiv n\pi/l_2,\ m = 1, 2, \ldots, M;\ n = 1, 2, \ldots, N.$

The tangential boundary conditions are satisfied on an average (see in this sense Librescu and Chang, 1992, 1993; Librescu and Lin, 1996; Librescu, 1975). To this end, the potential function $\psi$ is represented as:

$$\psi(x_\alpha, t) = \psi_1(x_\alpha, t) - \tfrac{1}{2}[(x_2)^2 \mathscr{N}_{11} + (x_1)^2 \mathscr{N}_{22}]. \tag{48}$$

Here $\psi_1(\equiv \psi_1(x_\alpha, t))$ is a particular solution of eqn (38) determined in conjunction with eqns (47a), $\mathscr{N}_{11}$ and $\mathscr{N}_{22}$ denoting the normal edge loads (considered positive in compression), see e.g. Librescu (1975).

In the case when the shell is supported on the inner surface by a Winkler linear/non-linear foundation, the governing equation (41a) has to be considered in conjunction with eqn (44).

Following the procedure used e.g. in Librescu and Chang (1992, 1993), the displacement expansions given by eqn (46a) are substituted into eqn (38) and $\psi_1(x_1, x_2, t)$ is obtained by solving the resulting linear nonhomogeneous partial differential equation. The remaining governing equation, eqn (41a), is converted, via Galerkin's method, into a set of non-linear ordinary differential equations. This procedure yields the following non-linear ordinary differential equation governing the postbuckling behavior

$$A_{rs}\ddot{w}_{rs} + R_{rs}w_{rs} + \bar{p}_{rs}B_{rs} + P_1[w_{rs}, \mathring{w}_{rs}, L_{11}, L_{22}, K_1] + \hat{P}_1[w_{rs}, \mathring{w}_{rs}, \mathring{T}_{rs}, \overset{1}{T}_{rs}] + P_2[w_{rs}^2, \mathring{w}_{mn}] + P_3[w_{rs}^3, \mathring{w}_{mn}, K_3] = 0 \quad \overset{*}{\sum_{r,s}}. \tag{49}$$

The symbol $\overset{*}{\sum}_{r,s}$ indicates that in the associated expression there is no summation over the indices, $r$ and $s$, where $r = 1, 2, \ldots, M$ and $s = 1, 2, \ldots, N$. In eqns (49), $\hat{P}_1$, and $P_1$ are linear, while $P_2$ and $P_3$ are, quadratic, and cubic polynomials of the unknown modal amplitudes $w_{rs}$, respectively; their dependence on the various parameters is also indicated in the brackets. The coefficients $A_{rs}$, $B_{rs}$, and $R_{rs}$ are constants not displayed here that depend on the material and the geometric properties of the shell; $L_{11}(\equiv \mathscr{N}_{11} l_1^2/\pi^4 \mathscr{D})$ and $L_{22}(\equiv \mathscr{N}_{22} l_1^2/\pi^4 \mathscr{D})$ are the normalized forms of normal edge loads, $\bar{p}_{rs}(\equiv p_{rs} l_1^4/(\mathscr{D}h))$ the dimensionless lateral pressure amplitude, while $K_1(\equiv \bar{K}_1 l_1^4/\pi^4 D)$ and $K_3(\equiv \bar{K}_3 l_1^2/\pi^4 D)$ are dimensionless Winkler's foundation moduli.

The static counterpart of eqns (49) enables one to illustrate in the planes $(L_{11}, \delta + \delta_0)$, $(\mathring{T}, \delta + \delta_0)$ or $(\hat{p}, \delta + \delta_0)$ the non-linear behavior of geometrically imperfect flat and curved panels. In the case of compressed panels, another representation enabling one to correlate the theoretical findings with the experimental ones is depicted in the plane $(L_{11}, \Delta_1)$, where $\Delta_1$ denotes the average endshortening in the direction of the coordinate $x_1$, and is defined by $\Delta_1 = -1/(l_1/l_2)\int_0^{l_1}\int_0^{l_2} v_{1,1}\, \mathrm{d}x_1\, \mathrm{d}x_2$ which should be considered in conjunction with eqns (27), (35), (31), (47) and (46).

## 6. Vibrational behavior in the pre-postbuckling/limit ranges

Towards studying this problem, we will restrict our attention to small vibrations $\bar{\bar{w}}_{mn}(t)$ about the static equilibrium position identified by $\bar{w}_{mn}$ (see Librescu et al. 1996). In this case, the vibration amplitude can be represented as

$$w_{mn}(t) = \bar{w}_{mn} + \bar{\bar{w}}_{mn}(t), \tag{50}$$

where the time-dependent part $\bar{\bar{w}}_{mn}$ is considered small as compared to $\bar{w}_{mn}$ and $\mathring{w}_{mn}$, in the sense of

$$\bar{\bar{w}}^2_{mn} \ll (\bar{w}_{mn}, \mathring{w}_{mn}). \tag{51}$$

The dependence of the static part of eqns (50) (defining the mean equilibrium position of the shell) upon the compressive edge loads, lateral pressure and the thermal field can be determined from the governing equations [eqns (49)], by discarding the inertia terms. The equation of motion for small vibrations of the composite shell about this position can be obtained by substituting eqn (50) into eqns (49), where the order of magnitude stipulated by eqns (51) should be enforced.

In such a way, the equation of vibration about the equilibrium position is obtained as

$$A_{mn}\ddot{\bar{\bar{w}}}_{mn} + D_{mn}\bar{\bar{w}}_{mn}0, \quad \sum_{m,n} \tag{52}$$

where $D_{mn} \equiv D_{mn}(\bar{w}_{mn}, \bar{w}^2_{mn}, \bar{w}^3_{mn}, \mathring{w}_{mn}, p_{mn}, \mathring{T}_{mn}, \overset{1}{T}_{mn}\bar{K}_1, \bar{K}_3)$, the coefficient $A_{mn}$ containing all the information about the thermo-mechanical and geometrical properties of the structure.

Employment in eqn (51) of the representation $\bar{\bar{w}}_{mn}(t) = \tilde{w}_{mn}\exp(i\omega_{mn}t)$, $(i = \sqrt{-1})$, and keeping in mind that $\bar{w}_{mn}$ is obtainable from the static counterpart of eqn (49), eqn (52) provides the interaction between the vibration frequency and the compressive, lateral and thermal loads in the pre- and postbuckling ranges (for the perfect panels), and in the pre- and post-limit ranges (for the geometrically imperfect ones).

## 7. Numerical illustrations and discussion

A range of applications involving the non-linear response of simply supported curved panels exposed to thermomechanical loads is considered. Their role is to get a better understanding of the implications brought by the violation of shear traction continuity requirement. The considered panels exhibit a square planform projection (of the side lengths $l_1 = l_2 = l$), and consist of three layers, in which the constituent materials exhibit transversely-isotropic thermoelastic properties.

Unless otherwise stated, one assumes that the core layer is twice as thick as each of the face-layers. In addition, the elastic moduli and thermal compliance coefficients defined in terms of non-dimensional ratio, are displayed in Table 1.

The considered numerical data reflect the fact that the core layer is more shear-deformable than the face layers, a behavior which is commonly valid in sandwich-type constructions. Since the mass

Table 1
Thermoelastic characteristics for the facings and core of the three-layer laminate

| | $E/E'$ | $E/G'$ | $\lambda/\lambda'$ | $\lambda/E$ | $v$ |
|---|---|---|---|---|---|
| Faces | 5 | 10 | 1.4286 | $-1.15\times10^{-5}$ in/in/°F | 0.2 |
| Core | 2 | 30 | 1.21413 | $-4.8875\times10^{-5}$ in/in/°F | 0.2 |

density of layers is absorbed in the dimensionless frequency $\bar{\omega}^2$, this characteristic was not displayed in Table 1.

In the forthcoming presentations the indices $f$ and $c$ are intended to identify the affiliation of the quantities affected by these indices to the face and core layer, respectively.

Having in view that for the present analyzed problems the one-term approximation in the representation of $v_3$ results in the most critical conditions (see e.g. Refs 30 and 32), only mode (1, 1) in the bending deflection has been considered. Moreover, the initial imperfection $\mathring{v}_3$, pressure $p_3$ and temperatures $\overset{\circ}{T}$ and $\overset{1}{T}$ are represented in the same shape of mode (1, 1). For the sake of convenience the amplitudes $\delta_{11}(\equiv w_{11}/h)$, $\overset{\circ}{\delta}_{11}(\equiv \mathring{w}_{11}/h)$, $\overset{\circ}{T}_{11}$ and $\overset{1}{T}_{11}$ corresponding to the center of the panel ($x_1 = x_2 = l/2$), are denoted in the numerical illustrations as $\delta$, $\delta_0$, $\overset{\circ}{T}$ and $\overset{1}{T}$, respectively. In addition, the dimensionless expressions of pressure amplitude and fundamental frequency (squared) will be denoted in the numerical illustrations as $\hat{p}(=p_{11}l_1^4/\mathscr{D}h)$ and $\bar{\omega}^2(\equiv\omega^2 m_0 l_1^4/\pi^4\mathscr{D})$, respectively.

In the absence of any specification about the character of in-plane boundary conditions, freely-moveable edge conditions should be considered.

### *7.1. Influence of a thermomechanical loads on the non-linear response as predicted by the Models I and II*

In Figs 2a and b the static postbuckling response and frequency–temperature interaction of the geometrically perfect and imperfect ($\delta_0 = 0.01$) three-layer flat panels subjected to a pre-existent system of biaxial compressive edge loads (indicated by the ratio $L_R(\equiv \mathscr{N}_{22}/\mathscr{N}_{11}) = 0.1$ where $L_{11}$ is the dimensionless subcritical compressive edge load, $L_{11} = 0.75(L_{11})_{cr}$), and to a uniform through the panel thickness temperature rise was considered. Herein and in the forthcoming illustrations, $(L_{11})_{cr}$ denotes the dimensionless uniaxial buckling load of the geometrically perfect Kirchhoffean plate/shell counterpart.

For both the geometrically perfect and imperfect panels, Model I violating the shear traction interlaminar continuity condition underestimates the thermal load carrying capacity of the panel.

As concerns the implications of the violation of continuity requirement on the frequency–temperature interaction, Fig. 2b reveals that for the geometrically perfect panels, in the pre-buckling range, Model I underestimates the fundamental frequency. For the same case, it can be seen that the buckling temperature, corresponding to zero-valued frequency is underestimated by Model I. However, in the postbuckling range, Model I overestimates the fundamental frequency. The increase in the fundamental frequency above the buckling temperature is attributed to the change in the panel geometry that occurs after buckling, resulting in the increase of the overall panel stiffness.

Having in view that for this case, the increase of the overall stiffness within Model I occurs prior to that of the Model II, in the postbuckling range, Model I overpredicts the fundamental frequency. When an initial geometric imperfection is implied, the fundamental frequency is larger than that of the perfect panel counterpart. Moreover, in the case of the geometrically imperfect panels, the initial decay of the fundamental frequency is experienced over a more reduced temperature interval than in the case of the geometrically perfect panel, for which the fundamental frequency becomes zero-valued at the buckling temperature. After that slight decrease, a steep increase of the frequency

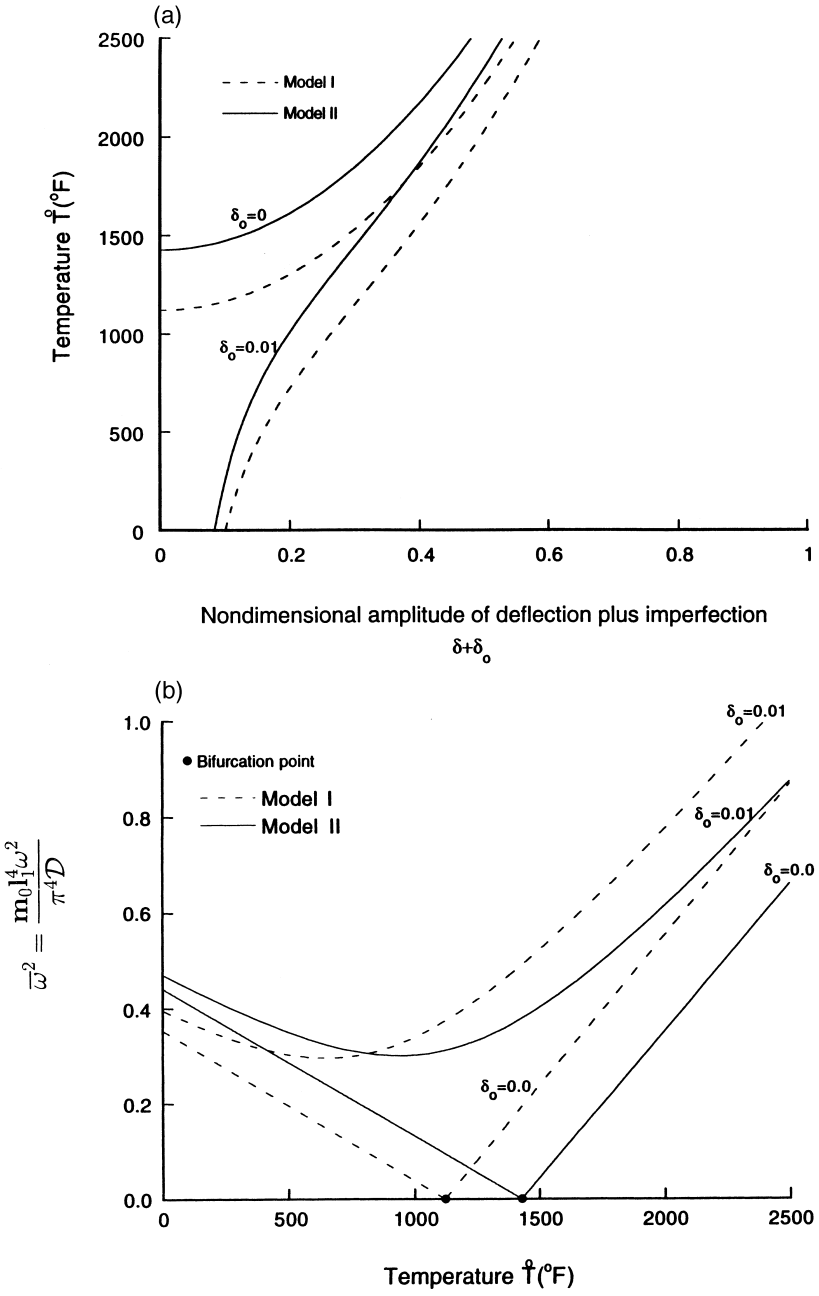


Fig. 2. (a) Non-linear response of geometrically perfect/imperfect flat panels subjected to a membrane temperature rise ($T_1 = 0$) and a pre-existent bi-axial compressive edge load, $L_R = 0.1$ and $L_{11} = 0.75\ (L_{11})_{cr}$, $l_1/l_2 = 1$, $l_1/h = 20$, $E_f = E_c$ (the remaining ones are being displayed in Table 1), as predicted by Models I and II. (b) Frequency–temperature interaction as predicted by Models I and II for the conditions and characteristics of the panel described in Fig. 2a.

with the increase of the temperature amplitude is experienced. In the latter temperature range, Model I overestimates the frequency predicted by Model II.

In Figs 3a and b, a similar scenario as in Figs 2a and b is considered. However, in this case, a thinner panel than in the previous case, and in addition, a core layer featuring a larger transverse shear stiffness than that of the face layers are considered. In these conditions, Fig. 3a reveals that Model I overestimates the thermal carrying capacity of both the geometrically perfect and imperfect panels, whereas from Fig. 3b it results that Model I associated with the perfect panel overestimates the frequencies in the prebuckling range. The same trend is valid in the case of geometrically imperfect panel, but over a limited range of the temperature rise, beyond which is underestimates the frequencies.

From Figs 3a and b it becomes also apparent that, in contrast to the results highlighted in Figs 2a and b, the predictions provided by Models I and II are much closer to each other. This is due to the fact that in this case the panel is much thinner than in the previous case, and as a result, the static continuity requirement plays a much less important role.

In Figs 4a and b, the non-linear response of a geometrically perfect circular cylindrical panel exposed to a dimensionless pre-existent uniaxial compression $L_{11} = 0.75\ (L_{11})_{cr}$, and to a thicknesswise temperature gradient is highlighted. It is supposed that the unloaded straight edges are either free-moveable ($\lambda_2 = 0$) or immoveable ($\lambda_2 = 1$).

From Fig. 4a and its counterpart, Fig. 4b, depicted in the plane $(\overset{\circ}{T}, \Delta_1)$, it results that Model I overestimates the limit temperature and the severity of the snap through jump as compared to those predicted by Model II. The results also reveal that for the same case, the classical Love–Kirchhoff shell model, although predicts a lower limit temperature than that provided by the higher-order shell theories, underestimates the severity of the snap-through jump. In the case of moveable straight edges ($\lambda_2 = 0$), a benign non-linear temperature-deflection dependence, in the sense of a monotonous increase of the deflection with the rise of the temperature field is experienced. The results associated with this case reveal that the predictions supplied by Model I underestimate the temperature carrying capacity as provided by Model II. At the same time, it results that in this case, the CLT overestimates the load carrying capacity as predicted by any of the shear-deformable theories considered in this study. The results of this graph also reveal that the first order shear deformation theory with $K^2 = 5/6$ provides the closest results to the ones predicted by the Model II. In a different context (see e.g. Librescu and Schmidt, 1991; Schmidt and Librescu, 1994), where a different theory of laminated shells fulfilling the continuity of interlaminar shear tractions was described, a similar conclusion was conjectured. From Fig. 4b it is also seen that in both cases of moveable and immoveable straight edges, Model I overestimates the endshortening when compared with that predicted by Model II. At the same time, the classical shell theory invariably underestimates the endshortening.

In Figs 5a and b, a very thin ($l_1/h = 100$) three-layer spherical cape exposed to a pre-existent temperature field $T_u = 70^\circ\text{F}$ and $T_b = 700^\circ\text{F}$ and a lateral pressure rise was considered. It is supposed that the edges $x_1 = 0, l_1$ and $x_2 = 0, l_2$ feature various degrees of tangential edge restraint, in the sense that for these edges, $0 \leqslant \lambda_1 \leqslant 1$ and $0 \leqslant \lambda_2 \leqslant 1$, respectively. The results reveal that for such a thin panel, Models I and II provide almost identical non-linear response behaviors. In addition, the results highlight the dramatic effects played by tangential edge constraints upon the panel load carrying capacity. From this graph it is evident that for fully immoveable edges $x_1 = 0$, $l_1$ and $x_2 = 0$, $l_2$ ($\lambda_1 = \lambda_2 = 1$), a maximum load carrying capacity is obtained. However, this

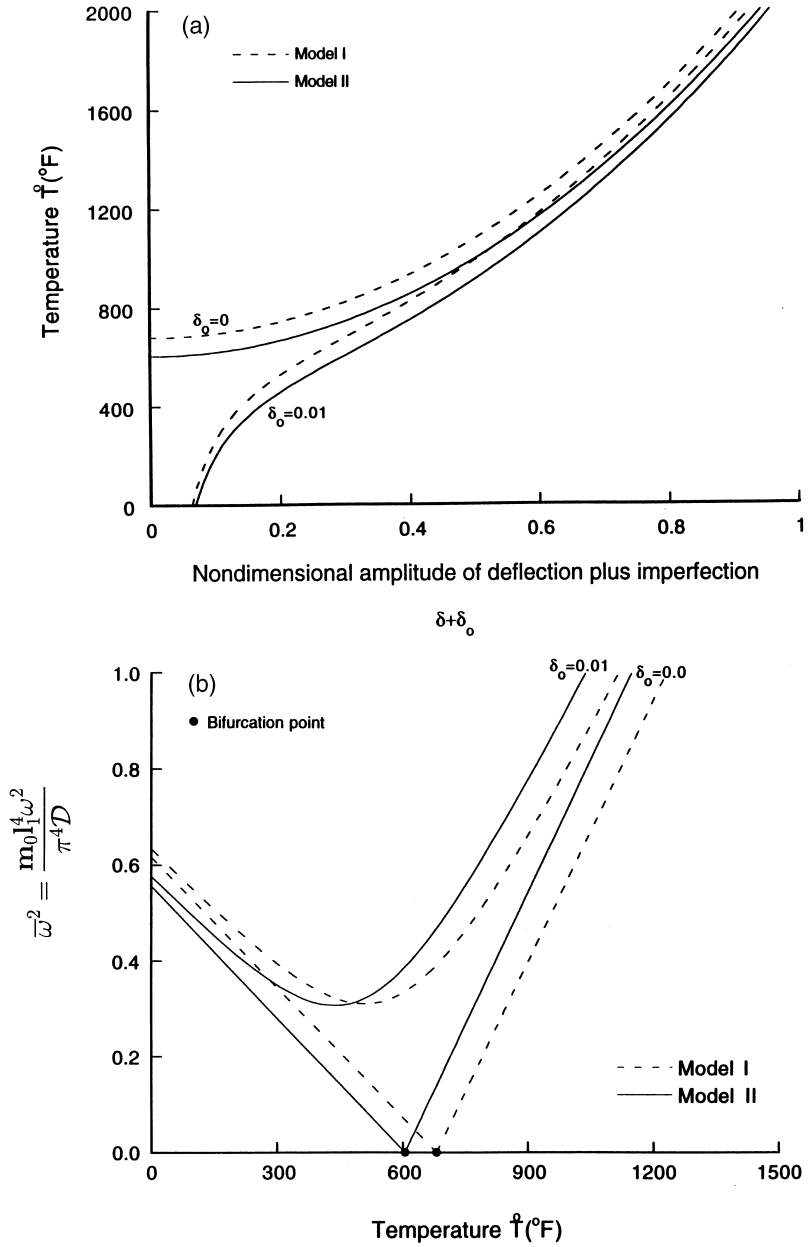


Fig. 3. (a) Predictions by Models I and II of the non-linear response of geometrically perfect/imperfect panels subjected to a membrane temperature rise ($T_1 = 0$) and a pre-existent bi-axial compressive edge load $L_R = 0.1$ and $L_{11} = 0.75$ $(L_{11})_{cr}$ $(l_1/l_2 = 1, l_1/h = 35,\ (E/G')_c = 10,\ (E/G')_f = 30,\ E_f = E_c$, the remaining ones being displayed in Table 1). (b) Frequency–temperature interaction in the conditions and panel characteristics as described in Fig. 3a, as predicted by Models I and II.

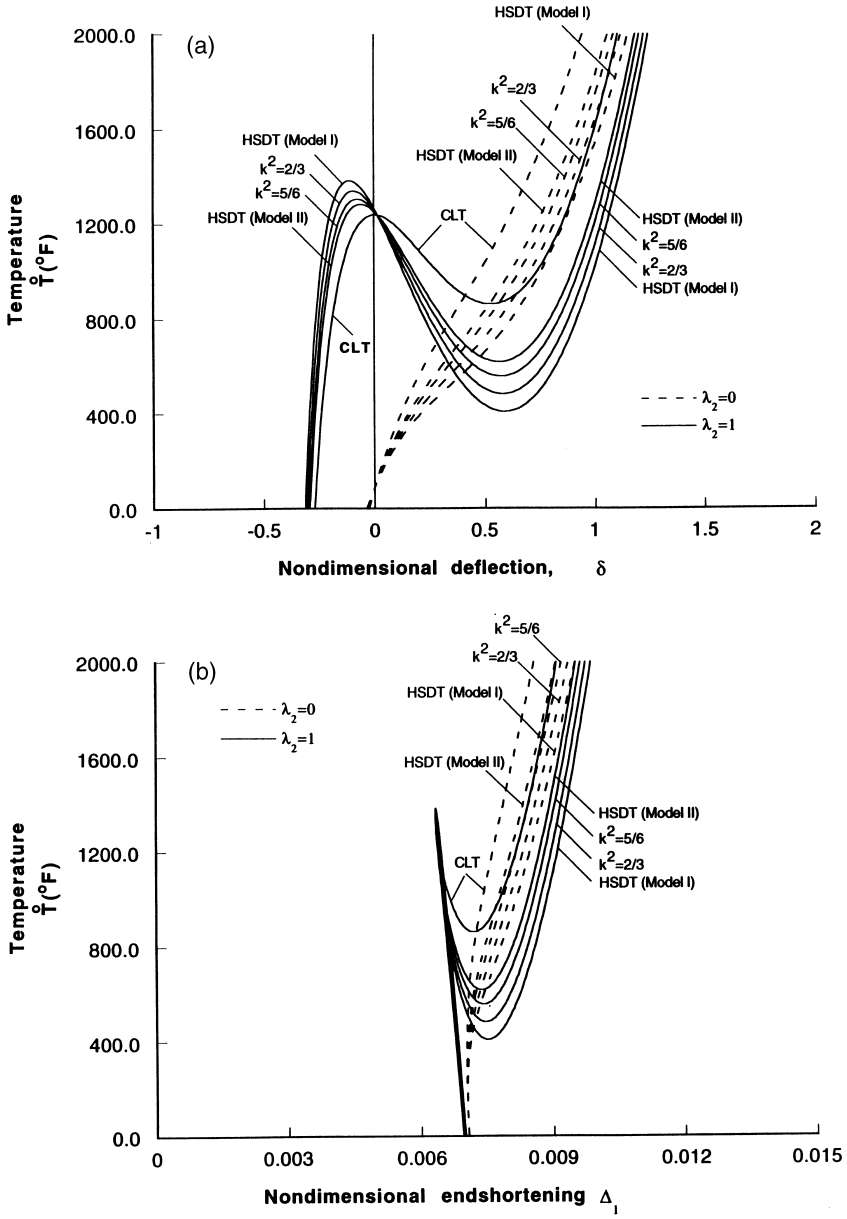


Fig. 4. (a) Non-linear response of an initially compressed three-layer circular cylindrical panel ($L_{11} = 0.75\ (L_{11})_{cr}$), subjected to a through-the-thickness temperature gradient ($l_1/R_l = 0$, $l_2/R_2 = 0.1$, $l_1/h = 25$, $l_1/l_2 = 1$, the thermoelastic properties being displayed in Table 1). The comparisons have concern the HSDT as per the Models I and II, FSDT with consideration of $K^2 = 5/6$ and 2/3, and CLT. (b) The counterpart of Fig. 4a displayed in the $(\mathring{T}, \Delta_1)$ plane.

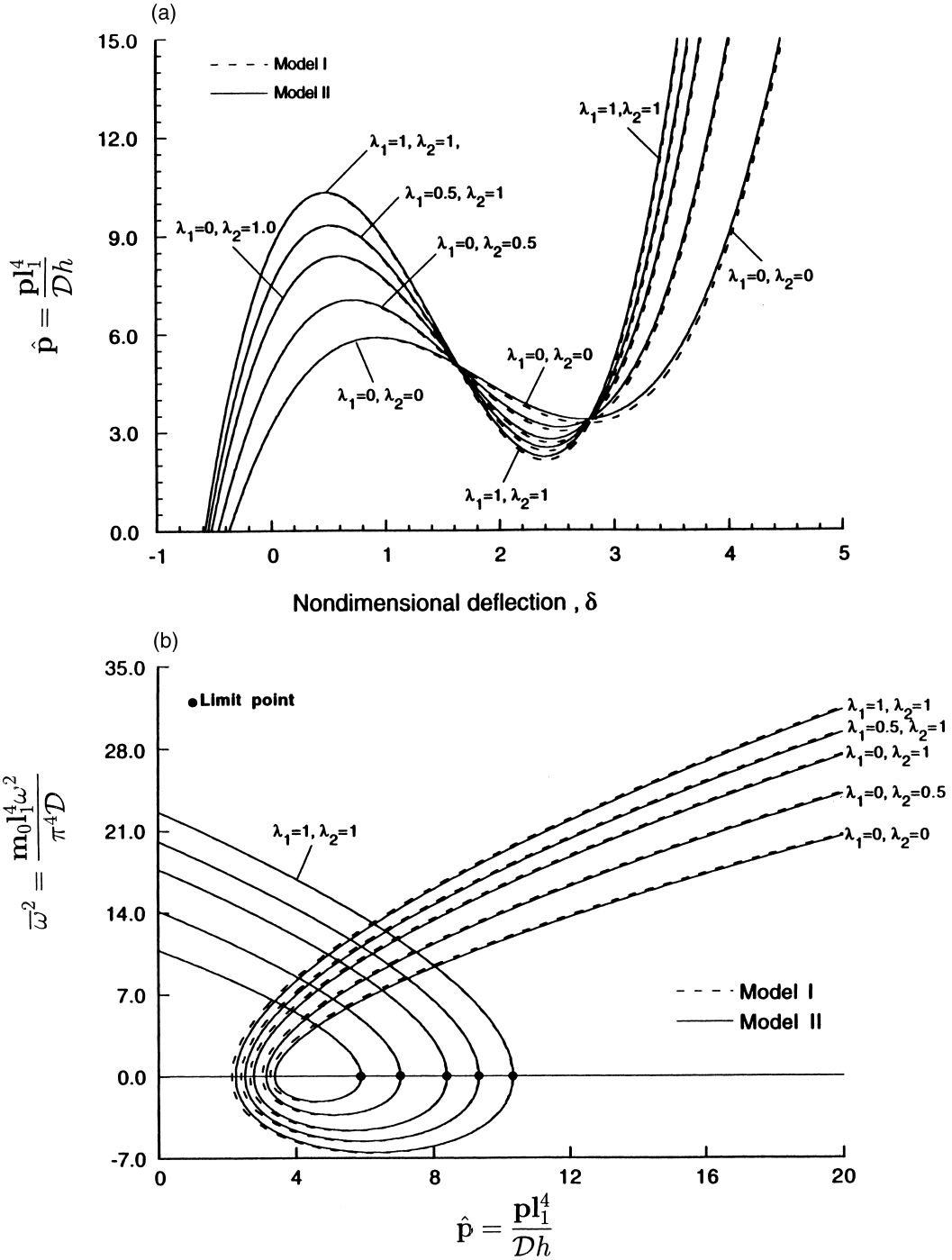


Fig. 5. (a) Non-linear response of three-layer spherical cape exposed to a pre-existent thicknesswise temperature ($T_u = 70°F$ and $T_b = 700°F$) and a lateral pressure rise, as predicted by Models I and II. The panel edges feature various degrees of tangential edge restraints. In addition to the thermomechanical characteristics displayed in Table 1, $l_1/h = 100$, $l_1/R_1 = l_2/R_2 = 0.1$; $t_c = 2t_f$, $l_1/l_2 = 1$; $E_f/E_c = 10$. (b) Frequency–pressure interaction for the panel described in Fig. 5a.

beneficial behavior can be associated with a very detrimental one, namely by a severe snap-through jump when the limit load is exceeded. It is also seen that for freely-moveable edges all around the contour ($\lambda_1 = \lambda_2 = 0$), the load carrying capacity is much lower, as compared to that occurring in the previous case. However, this latter behavior is compensated by the occurrence of a much less severe snap-through jump as compared to that in the previous case. Figure 5b representing the dynamic counterpart of Fig. 5a, reveals a similar trend, in the sense that for $\lambda_2 = \lambda_1 = 1$ and $\lambda_1 = \lambda_2 = 0$, maxima and minima fundamental frequencies in both the pre- and post-limit load ranges are experienced, respectively. For intermediate conditions of the immovability/moveability of the opposite edges, intermediate static and dynamic response behaviors from the point of view of the magnitude of frequencies and of the intensity of the dynamic snap-through jump, are experienced.

In Figs 6a and b, a plot of the behavior described within the Models I and II, of a geometrically imperfect ($\delta_0 = 0.1$) circular cylindrical three-layer panel of moderate thickness ($l_1/h = 10$), subjected to an increasing uniaxial compressive load is considered. It is assumed the straight edges feature various degrees of tangential edge constraints, implying that on these edges $0 \leqslant \lambda_1 \leqslant 1$.

From Fig. 6a it appears that Model I, while underpredicting the load carrying capacity of the panel, it experiences for $\lambda_2 = 1$, likewise Model II, a limit load, beyond which, a snap-through buckling is followed. From the plot, it is also evident that Model I underpredicts the severity of the snap-through jump as compared to that predicted by Model II.

The dynamic counterpart of this graph, Fig. 6b, depicting the fundamental frequency–compressive load interaction reveals a similar trend, in the sense that Model I, underestimates the fundamental frequency in the pre-limit load range, underestimates the severity of the dynamic snap-through when the compressive loads increase beyond the limit loads corresponding to the considered tangential edge constraints, and overestimates the fundamental frequency in the post-limit load range.

However, in the case shown in Fig. 7 which corresponds also to a moderately thick ($l_1/h = 10$) three-layer circular cylindrical panel featuring a smaller initial geometric imperfection ($\delta_0 = 0.05$), than in the previous case, both Models I and II predict, qualitatively, similar non-linear behaviors under the variation of the degree of the tangential edge constraint. As it can be seen from this graph, Model I slightly overpredicts the load carrying capacity. At the same time, one can observe that for $\lambda_2 = 1$ one obtains for both models the same benign non-linear response, while corresponding to $\lambda_2 = 0.36$ for Model I, and to $\lambda_2 = 0.41$ for Model II, a buckling bifurcation can be experienced. Moreover, in these cases, for compressive edge loads larger than those corresponding to the buckling bifurcation, a less severe snap-through jump is predicted by Model I as compared to that predicted by the more exact, Model II.

### *7.2. Influence of linear/non-linear Winkler's elastic foundation on non-linear response predicted by Models I and II*

Figure 8a depicts the non-linear response of a geometrically perfect circular cylindrical three-layer panel, of moderate thickness ($l_1/h = 10$), resting on a linear Winkler foundation ($K_3 = 0$), and uniaxially compressed by the edge load $L_{11}$. The results confirm the conclusion highlighted in Ref. 11, according to which the increase of the linear foundation modulus results in the increase of both the buckling bifurcation and of the load-carrying capacity. The results also reveal that

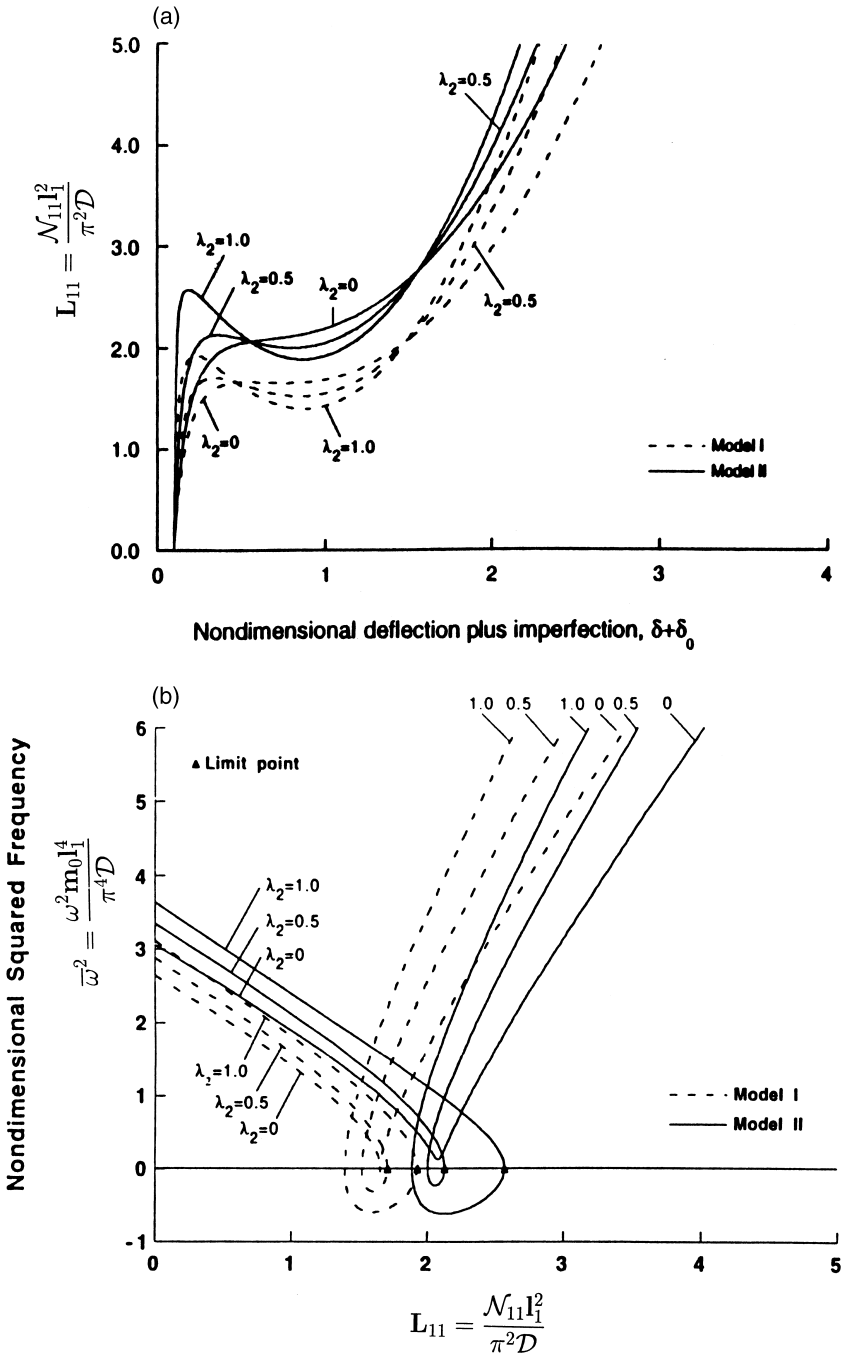


Fig. 6. (a) Comparison of predictions as provided by Models I and II on non-linear response of a circular cylindrical panel subjected to compressive loads applied on its curved edges, its straight edges experiencing various degrees of tangential edge constraint ($l_1/h = 10$, $l_1/R_1 = 0$, $l_2/R_2 = 0.5$, $t_c/t_f = 5$, $(E/G')_f = 15$, $(E/G')_c = 30$, $E_f = 5E_c$, $\delta_0 = 0.1$, $\lambda_1 = 0$). The remaining data are provided in Table 1. (b) Fundamental frequency (squared)-compressive edge load interaction as predicted by Models I and II for the case described in Fig. 6a.

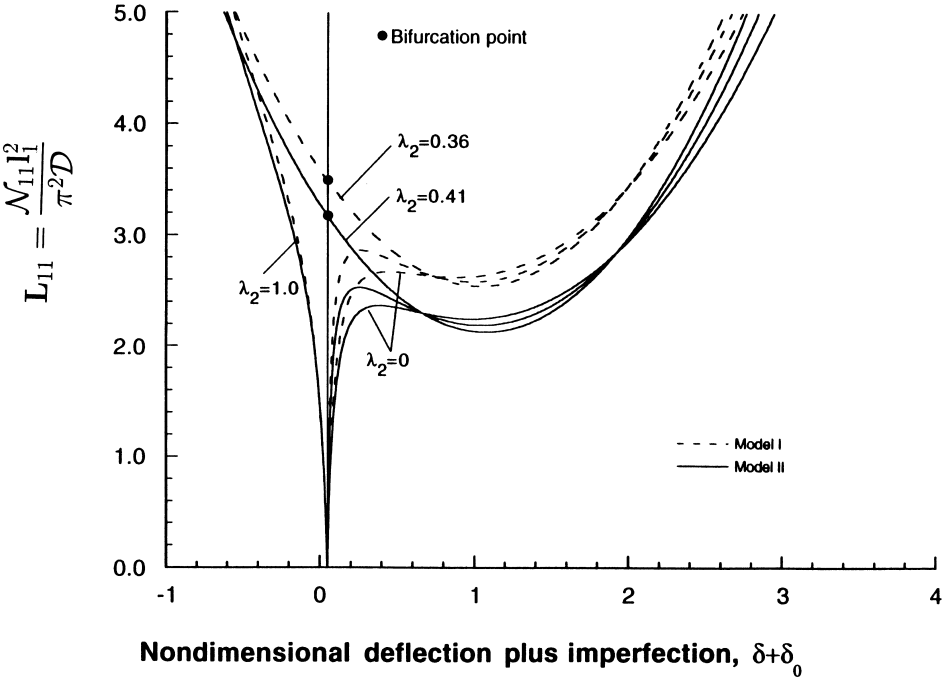


Fig. 7. Postbuckling response of circular cylindrical panels subjected to uniaxial compressive edge loads as predicted by Models I and II. Herein $l_1/h = 10$, $l_1/R_1 = 0$, $l_2/R_2 = 0.6$; $t_c/t_f = 5$, $(E/G') = 60$; $E_f = 10E_c$, $\delta_0 = 0.05$, $\lambda_1 = 0$. Various degrees of edge constraints on $x_2 = 0, l_2$.

Model I underestimates the beneficial effect played by the linear foundation characteristic upon the load carrying capacity. In addition Model I reveals less sensitivity to the variation of $K_1$ as compared to Model II, the differences between the two model predictions becoming more significant as the linear foundation modulus increases. Similar conclusions can be inferred from Fig. 8b depicting the frequency–compressive edge load interaction, in the sense that for small $K_1$ values, the frequency predictions provided by the two models are rather close to each other. However, with the increase in $K_1$, significative differences between the predictions of the two models occur.

The effect of the non-linear Winkler's foundation modulus $K_3$ upon the postbuckling response of geometrically imperfect circular cylindrical panel uniaxially compressed on the curved edges is presented in Fig. 9a. The results reveal that the non-linear foundation characteristic affects only the postbuckling behavior. In this respect, it should be observed that the increase of the hardening ($K_3 > 0$) non-linear foundation characteristics yields a reduction of the intensity of the snap-through buckling and even its elimination. It should be observed that in the case of the non-linear hardening type foundation ($K_3 > 0$), Model I underpredicts the load carrying capacity, while, in the case of the softening type foundation ($K_3 < 0$), it overpredicts the load carrying capacity.

From Fig. 9b depicting the endshortening as a function of the increase of the uniaxial compressive load, it becomes apparent that for hardening type foundation, for the same compressive load, Model I overestimates the endshortening, while for softer-type foundation it underestimates it.

Figure 9c represents the frequency–load interaction counterpart of Fig. 9a. The results reveal

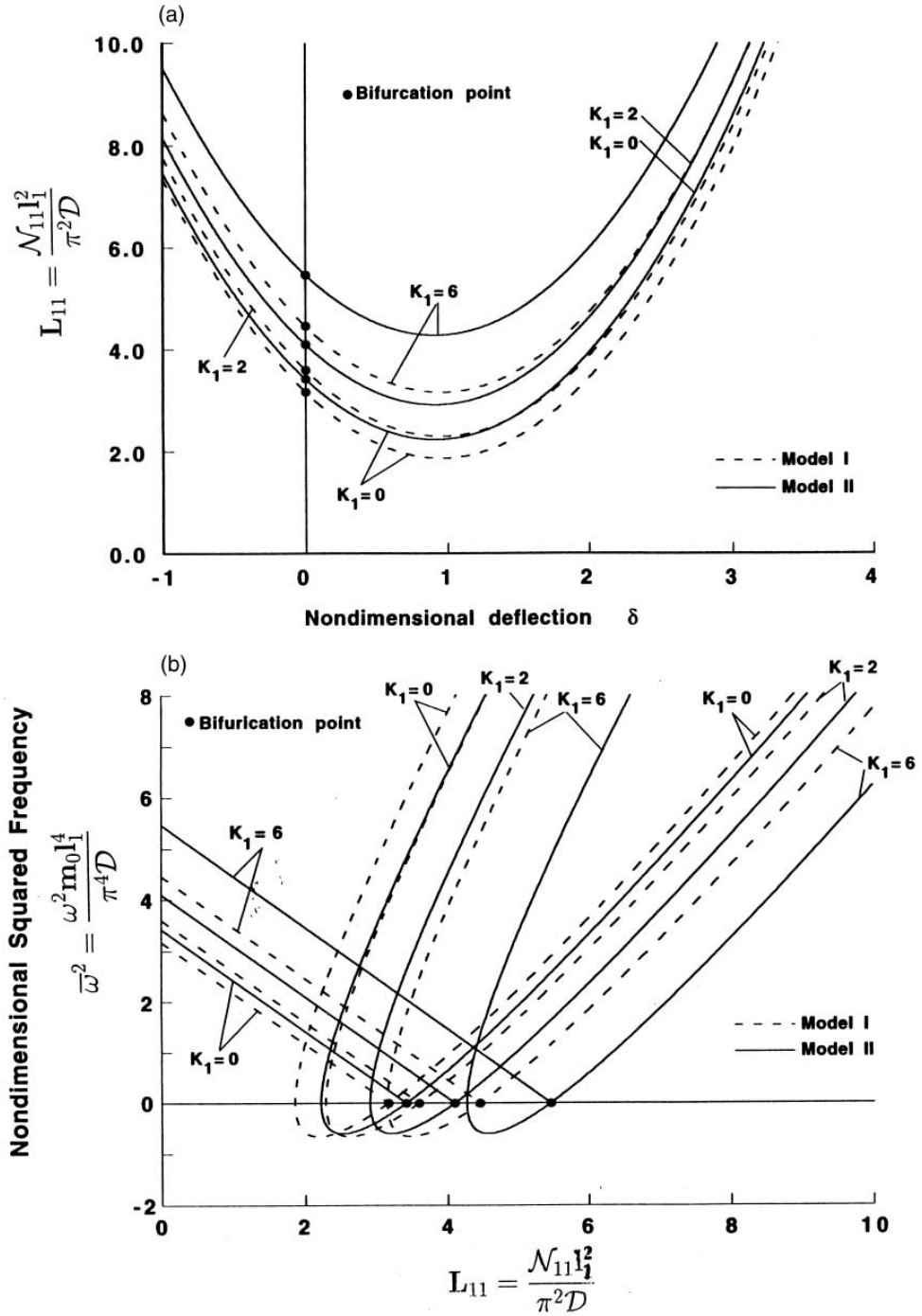


Fig. 8. (a) Influence of the linear Winkler's foundation modulus as predicted by the Models I and II on the non-linear response of a uniaxially compressed circular cylindrical panel ($l_1/h = 10$, $l_1/R_1 = 0$, $l_2/R_2 = 0.5$, $t_c/t_f = 4$, $(E/G')_f = 10$; $(E/G')_c = 50$; $E_f = E_c$. (b) Influence of the foundation linear Winkler's foundation modulus as predicted by Models I and II on frequency–compressive edge load interaction, for the case described in Fig. 7a.

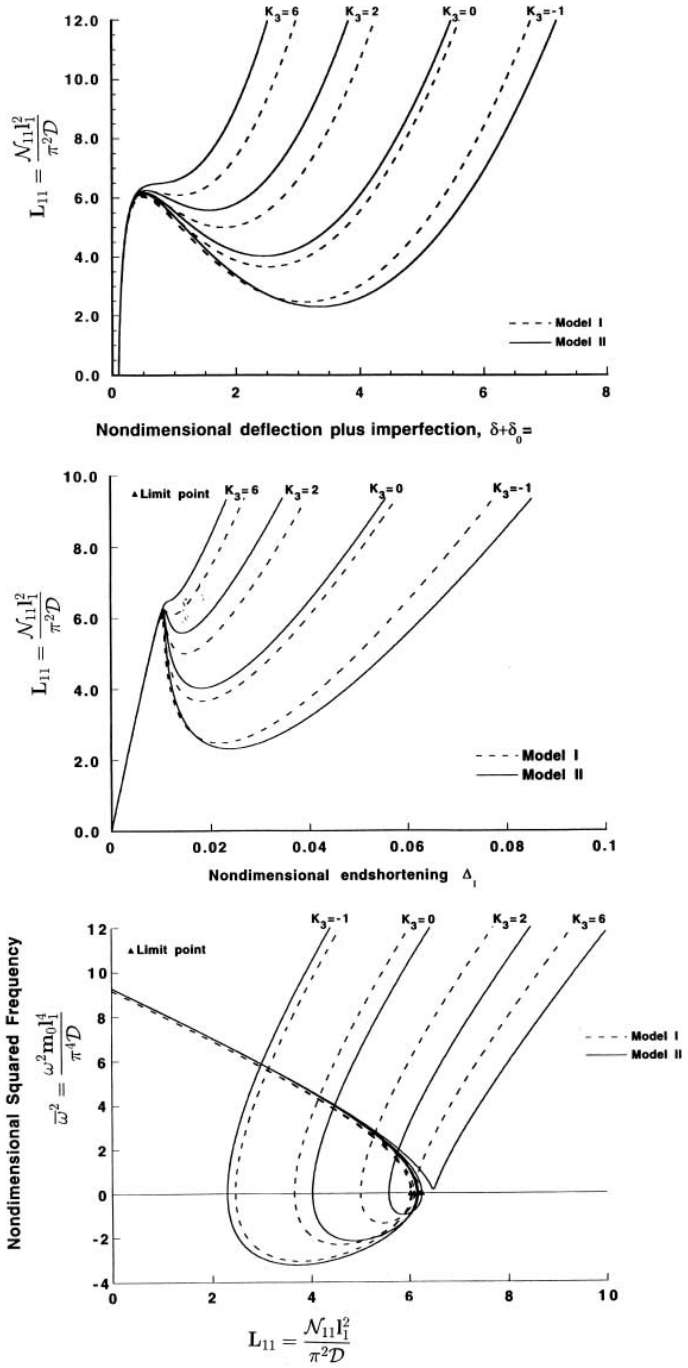


Fig. 9. (a) Influence of the cubic Winkler's foundation modulus as predicted by Models I and II, on the non-linear response of an imperfect ($\delta_0 = 0.1$) circular cylindrical panel subjected to uniaxial compressive edge loads ($l_1/h = 30$, $l_1/R_1 = 0$, $l_2/R_2 = 0.6$, $t_c/t_f = 2$, $E_f = 10E_c$, $K_1 = 0$, the remaining data being provided in Table 1). (b) Compressive edge load-end shortening dependence of the case described in Fig. 9a. (c) Fundamental frequency–compressive edge load interaction for the case described in Fig. 9b.

again the fact that $K_3$ influences solely the post-limit behavior. The highly beneficial effect of a hardening type foundation on the frequency–load interaction, in the sense of alleviating the dynamic snap-through jump, or eliminating it altogether (for $K_3 = 6$), becomes also evident from this graph. At the same time, one can remark that for soft-type foundation, in the post-limit range, Model I underpredicts the fundamental frequency while for hardening-type foundation, it overpredicts it.

### 7.3. *Influence of the thickness,* $t_c/t_f$ *and transverse-shear* $G'_c/G'_f$, *ratios on frequency–compressive edge load interaction as predicted by Models I and II*

Finally, in Figs 10 and 11 the influence of the relative thickness $t_c/t_f$ and transverse shear moduli of the core and face layers, $G'_c/G'_f$, on the frequency–compressive edge load interaction, as predicted by Models I and II is highlighted. In Fig. 10 the case of a slightly imperfect ($\delta_0 = 0.01$) three layer circular cylindrical panel ($l_1/R_1 = 0; l_2/R_2 = 0.6$) of moderate thickness ($l_1/h = 10$), subjected to uniaxial compressive edge loads is considered.

The results reveal that in the case of a single layer panel constituted either of the core layer ($t_c/t_f = \infty$), or of the face layers ($t_c/t_f = 0$), the two models provide, as it should be, identical results for each of these two cases. For values of the thickness ratio $t_c/t_f \neq 0, \infty$, until a certain value of the ratio ($t_c/t_c = 10$), Model I overestimates the frequencies in the pre-limit range, and under-

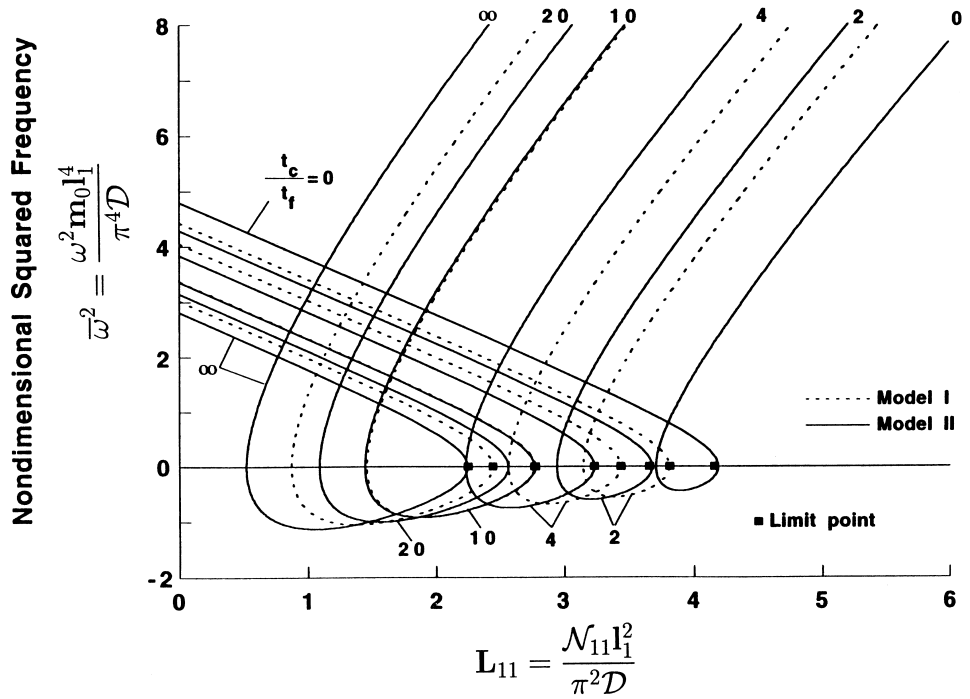


Fig. 10. Influence of the thickness ratio $t_c/t_f$ on the frequency–compressive edge load interaction of geometrically imperfect ($\delta_0 = 0.01$) circular cylindrical panels ($l_1/R_1 = 0$, $l_2/R_2 = 0.6$) of moderate thickness ($l_1/h = 10$), characterized by $(E/G')_f = 3$; $(E/G')_c = 60$; $E_f = E_c$, as predicted by Models I and II.

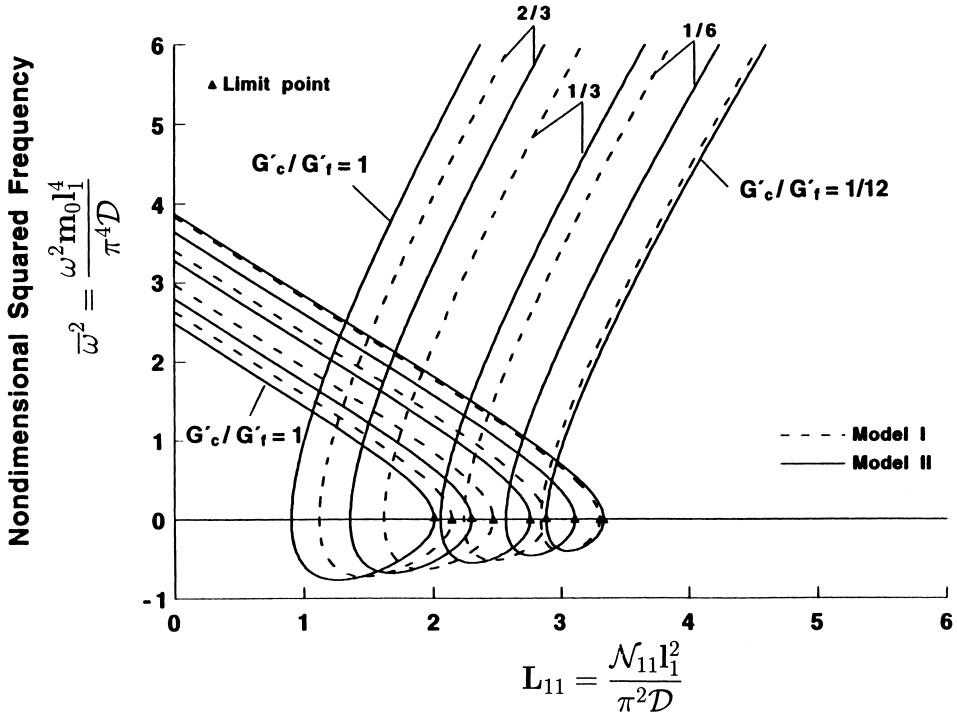


Fig. 11. Influence of the ratio $G_c'/G_f'$ of transverse shear moduli on the frequency–compressive edge load interaction of geometrically imperfect ($\delta_0 = 0.01$) circular cylindrical panels ($l_1/R_1 = 0$, $l_2/R_2 = 0.5$) of moderate thickness ($l_1/h = 10$), characterized by $(E/G')_c = 60$, $E_f = E_c$, as predicted by Models I and II.

estimates those ones in the post-limit range. Moreover, the result reveal that with the increase of the core thickness in the detriment of that of the faces, a continuous increase of the intensity of the dynamic snap-through jump occurring when the compressive load transcends the limit load is experienced. This trend is due to the fact that with the increase of the core thickness, which in this case, features a larger transverse shear flexibility than the faces, an overall increase of the transverse shear flexibility of the structure is experienced. Moreover, as a by-product, Fig. 10 reveals that with the increase of the core thickness in the detriment of that of faces, a continuous decrease of the limit loads occurs. At the same time, as is readily seen, with the increase of the core thickness until that value corresponding $t_c/t_f = 10$, Model I underestimates the limit load, while for $t_c/t_f > 0$, the opposite trend becomes valid.

Figure 11 highlights the effects played by the transverse shear flexibility characteristics of face layers relative to that of the core, measured in terms of the ratio $G_c'/G_f'$, as predicted by the Models I and II. For this case, the core layer features a high transverse shear flexibility ($(E/G')_c = 60$). The results of this plot reveal that Models I and II feature strong sensitivities to the variation of $G_c'/G_f'$. In addition, it is evident that with the decrease of transverse shear flexibilities of the faces as compared to that of the core, an increase of the frequencies in the pre-limit load ranges is experienced.

In this graph, this extreme case occurs for $G_c'/G_f' = 1/12$. The other extreme case corresponding

to $G'_c/G'_f = 1$, yields the lowest frequency in the pre-limit load range. For these two cases, Models I and II provide almost identical results. However, for intermediate values of $G'_c/G'_f$, the results reveal that Model I underestimates the frequencies in the pre-limit range, whereas in the post-limit range an opposite trend becomes valid. From the same graph it becomes apparent that with the decrease of the transverse shear stiffness of the faces as compared to that of the core, a decrease of the limit load and an increase of the severity of the dynamic snap-through jump which occur when the limit-load is exceeded, can be featured. In the case of the core featuring lower transverse shear flexibility, the results not displayed here (for the static non-linear response see Librescu et al., 1997, Fig. 8), reveal that within Model I, there is a much lower sensitivity of the variation of frequencies with the variation of the ratio $G'_c/G'_f$, as compared to that experienced within Model II.

Moreover, with the increase of the transverse shear modulus of the core as compared to that of the faces, the disagreement between predictions provided by the Models I and II tends to further increase.

## 8. Conclusions

A number of results highlighting the implications brought by the non-fulfilment of the shear traction continuity requirement upon the static and dynamic non-linear behavior of laminated flat and curved panels exposed to thermomechanical loadings have been presented.

Toward the end of accomplishing such a study, a simple geometrically non-linear model of laminated shells (referred to as Model II), fulfilling both the kinematic and shear traction interlaminar continuity conditions, as well as the ones postulating the absence of shear tractions on the external boundary surfaces of the panel, has been developed. The results reveal that, depending upon the relative transverse shear flexibility featured by the materials of the core and face layers, or of their relative thickness, the violation of the interlaminar shear traction continuity requirement, yields under/overestimation of the load carrying capacity of the panel or of the vibration frequencies.

In the same context, such a violation can result also in under/overpredictions of the intensity of the static/dynamic snap-through jump.

Depending upon the degree of the variation of transverse shear flexibilities and of the thicknesses of contiguous layers featuring larger transverse shear flexibility ratios, the resulting implications can be extremely significant.

Such over/underpredictions obtained within the model violating the interlaminar shear traction continuity requirement can be even exacerbated in some instances involving the presence of tangential edge constraints or the existence of a linear/non-linear elastic foundation.

It was also shown that in the case of very thin laminated shells, the fulfilment/violation of the interlaminar shear traction continuity requirement becomes redundant, in the sense that the predictions based on the two models become almost identical.

Another result concerns the classical Love–Kirchhoff model, which in the most general cases, overestimates the load carrying capacity of panels, as well as the vibration frequencies, and underestimates the intensity of the snap-through jump.

The results obtained in this study which complement the ones obtained previously in Librescu and Lin (1996) and Librescu et al. (1997), underline the fact, that in order to obtain more exact results on the thermomechanical load carrying capacity of structures and on their vibration frequencies, a structural model fulfilling all the continuity requirements should be used. In addition,

in studies involving determination of failure conditions in the postbuckling range of laminated constructions, wherein prediction of local response characteristics is of prime importance, only structural models fulfilling such continuity requirements would be able to supply reliable results in this respect.

It should be mentioned that all these conclusions concern the case of a perfectly interlaminar bonding between the contiguous layers of the panel. However, when this is not the case, i.e. when a damage of the interlaminar bonding is experienced yielding the possibility of the relative sliding of two contiguous layers of the laminate or of multiple delaminations, pertinent considerations in the modeling of laminated composite structures should be taken. Theoretical studies on this matter have been accomplished very recently, and assessments of the implications induced by such bonding imperfections can be found in Schmidt and Librescu (1996), Cheng et al. (1996, 1997a, b), Di Sciuva et al. (1997), Icardi et al. (1997) and Chattopadhyay and Gu (1994, 1996a, b).

**Acknowledgements**

One author of this paper (L. Librescu) acknowledges with gratitude partial support of this research by NATO Grant, CRG 960118. Both authors express their deep appreciation to Drs J. H. Starnes Jr and M. P. Nemeth of NASA Langley Research Center, Hampton, VA for stimulating technical discussions during the work accomplished within the NASA Grant NAG-1-1300.

**Appendix 1: Expression of anisotropic stiffness quantities**

$$\mathscr{D}^{\alpha\beta\omega\rho} = \frac{2}{3}\left[\tilde{E}^{\alpha\beta\omega\rho}_{\langle m+1\rangle}h^3_{m+1} + \sum_{r=1}^{m}\tilde{E}^{\alpha\beta\omega\rho}_{r}(h^3_r - h^3_{r+1})\right]$$

$$\mathscr{T}^{\alpha\beta\omega\rho} = \tilde{E}^{\alpha\beta\pi\rho}_{\langle m+1\rangle}J^{\langle m+1\rangle}_3 + \sum_{r=1}^{m}\tilde{E}^{\alpha\beta\omega\rho}_{\langle r\rangle}J^{\langle r\rangle}_4$$

$$\mathscr{L}^{\alpha\beta\omega\rho} = \frac{4}{3}\left[\tilde{E}^{\alpha\beta\lambda\rho}_{\langle m+1\rangle}F^{\langle m+1\rangle}_{\lambda 3\mu 3}A^{\mu 3\omega 3}_{(m+1)}h^3_{m+1} + \sum_{r=1}^{m}E^{\alpha\beta\lambda\rho}_{\langle r\rangle}F^{\langle r\rangle}_{\lambda 3\mu 3}A^{\mu 3\omega 3}_{(r)}(h^3_r - h^3_{r-1})\right]$$

$$\mathscr{S}^{\alpha\beta\gamma\rho} = 2\sum_{r=1}^{m}\tilde{E}^{\alpha\beta\omega\rho(r)}_{\langle r\rangle}\Omega^{\gamma}_{\omega}(h^2_r - h^2_{r-1})$$

$$\mathscr{K}^{\alpha 3\omega 3} = 2\left\{E^{\alpha 3\omega 3}_{\langle m+1\rangle}J^{\langle m+1\rangle}_1 + A^{\alpha 3\omega 3}_{(m+1)}h_{m+1} + \sum_{r=1}^{m}[E^{\alpha 3\omega 3}_{\langle r\rangle}J^{\langle r\rangle}_2 + A^{\alpha 3\omega 3}_{(r)}(h_r - h_{r-1})\right\},$$

$$\mathscr{F}^{\alpha\beta\omega\rho} = 2\left\{\tilde{E}^{\alpha\beta\omega\rho}_{\langle m+1\rangle}h_{m+1} + \sum_{r=1}^{m}\tilde{E}^{\alpha\beta\omega\rho}_{\langle m+1\rangle}(h_r - h_{r-1})\right\}$$

$$\Lambda^{\alpha\beta} = 2\left\{\tilde{\lambda}^{\alpha\beta}_{\langle m+1\rangle}h_{m+1} + \sum_{r=1}^{m}\tilde{\lambda}^{\alpha\beta}_{\langle r\rangle}(h_r - h_{r-1})\right\}$$

$$\Pi^{\alpha\beta} = \frac{2}{3}\left\{\tilde{\lambda}^{\alpha\beta}_{\langle m+1\rangle}h^3_{m+1} + \sum_{r=1}^{m}\tilde{\lambda}^{\alpha\beta}_{\langle r\rangle}(h^3_r - h^3_{r-1})\right\}.$$

In addition

$$J_0 \equiv \int_0^{x^3} f(x^3)\,\mathrm{d}x^3;$$

$$J_1^{\langle m+1\rangle} = \int_0^{h_{m+1}} f(x^3)\,\mathrm{d}x^3;$$

$$J_2 = \int_{h_{m+1}}^{h_m} f(x^3)\,\mathrm{d}x^3;$$

$$J_3^{\langle m+1\rangle} = \int_0^{h_{m+1}} J_0 x^3\,\mathrm{d}x^3;$$

$$J_4 = \int_{h_{m-1}}^{h_m} J_0 x^3\,\mathrm{d}x^3.$$

In these equations, $h_r$ denotes the distance from the shell mid-surface to the upper surface of the $r$th layer (see Fig. 1).

## Appendix 2: Transversely-isotropic specialized counterparts of stiffness quantities

$$A_{(r)}^{\alpha 3\omega 3} \Rightarrow -a^{\alpha\omega}A(r)$$

where

$$A_{(r)} = \sum_{i=2}^{r} f(h_i)(G'_{\langle i\rangle} - G'_{\langle i-1\rangle})$$

$${}^{(r)}\Omega_{\lambda}^{\gamma} \Rightarrow -\frac{1}{4}\delta_{\lambda}^{\gamma}\Omega_{(r)}$$

where

$$\Omega_{(r)} = \sum_{i=2}^{r} h_i\left(\frac{A_{(i)}}{G'_{\langle i\rangle}} - \frac{A_{(i-1)}}{G'_{\langle i-1\rangle}}\right).$$

$$\mathscr{D}^{\alpha\beta\omega\rho} \Rightarrow \mathscr{D} = \frac{2}{3}\left[\bar{E}_{\langle m+1\rangle}h_{m+1}^3 + \sum_{r=1}^{m}\bar{E}_{\langle r\rangle}(h_r^3 - h_{r-1}^3)\right]$$

$$\mathscr{L}^{\alpha\beta\omega\rho} \Rightarrow -\frac{1}{3}\left\{A_{(m+1)}\frac{G_{\langle m+1\rangle}}{G'_{\langle m+1\rangle}}\left[a^{\alpha\omega}a^{\beta\rho} + a^{\omega\rho}a^{\alpha\beta} + \frac{2v_{\langle m+1\rangle}}{1-v_{\langle m+1\rangle}}a^{\omega\rho}a^{\alpha\beta}\right]h_{m+1}^3 + \sum_{r=1}^{m}A_{(r)}\frac{G_{\langle r\rangle}}{G'_{\langle r\rangle}}\left[\left(a^{\alpha\omega}a^{\beta\rho} + a^{\omega\rho}a^{\alpha\beta} + \frac{2v_{\langle r\rangle}}{1-v_{\langle r\rangle}}a^{\gamma\rho}a^{\alpha\rho}\right)(h_r^3 - h_{r-1}^3)\right]\right\}$$

$$\mathscr{S}^{\alpha\beta\omega\rho} \Rightarrow -\frac{1}{2}\sum_{r=1}^{m} G_{\langle r\rangle}\Omega_{(r)}\left[a^{\alpha\omega}a^{\beta\rho}+a^{\omega\beta}a^{\alpha\rho}+\frac{2v_{\langle r\rangle}}{1-v_{\langle r\rangle}}a^{\omega\rho}a^{\alpha\beta}\right](h_r^2-h_{r-1}^2)$$

$$\mathscr{K}^{\alpha 3\omega 3} \Rightarrow \mathscr{K}a^{\alpha\omega}$$

where

$$\mathscr{K} = 2\left[G'_{\langle m+1\rangle}J_1^{\langle m+1\rangle}-A_{(m+1)}h_{m+1}+\sum_{r=1}^{m}(G'_{\langle r\rangle}J_2^{\langle r\rangle}-A_{(r)}(h_r-h_{r-1})\right]$$

$$\Lambda^{\alpha\beta} \Rightarrow \Lambda a^{\alpha\beta}; \quad \Pi^{\alpha\beta} \Rightarrow \Pi a^{\alpha\beta}$$

where

$$\Lambda = 2\left[\tilde{\lambda}_{\langle m+1\rangle}h_{m+1}+\sum_{r=1}^{m}\tilde{\lambda}_{\langle r\rangle}(h_r-h_{r-1})\right]$$

$$\Pi = \frac{2}{3}\left[\tilde{\lambda}_{\langle m+1\rangle}h_{m+1}^3+\sum_{r=1}^{m}\tilde{\lambda}_{\langle r\rangle}(h_r^3-h_{r-1}^3)\right].$$

$$\mathscr{F}^{\alpha\beta\omega\rho} \Rightarrow b(a^{\alpha\omega}a^{\beta\rho}+a^{\omega\beta}a^{\alpha\rho})+2ca^{\omega\rho}a^{\alpha\beta}$$

where

$$b = \left[G_{\langle m+1\rangle}h_{m+1}+\sum_{r=1}^{m}G_{\langle r\rangle}(h_r-h_{r-1})\right]$$

$$c = 2\left[\frac{G_{\langle m+1\rangle}v_{\langle m+1\rangle}}{1-v_{\langle m+1\rangle}}h_{m+1}+\sum_{r=1}^{m}\frac{G_{\langle r\rangle}v_{\langle r\rangle}}{1-v_{\langle r\rangle}}(h_r-h_{r-1})\right]$$

$$\mathscr{P}_{\alpha\beta\lambda\sigma} = \tilde{b}(a_{\alpha\lambda}a_{\beta\sigma}+a_{\lambda\beta}a_{\alpha\sigma})+2\tilde{c}a_{\lambda\sigma}a_{\alpha\beta}$$

where

$$\tilde{b} = \frac{1}{b}; \quad \tilde{c} = -\frac{c}{b(b+2c)}$$

$$\tilde{\Lambda}_{\pi\sigma} \Rightarrow \tilde{\Lambda}a_{\pi\sigma} \quad \text{where } \tilde{\Lambda} = -\frac{\Lambda}{b+2c}$$

$$\mathscr{T}_1 = 2\left(G_{\langle m+1\rangle}J_3^{\langle m+1\rangle}+\sum_{r=1}^{m}G_{\langle r\rangle}J_4^{\langle r\rangle}\right)$$

$$\mathscr{T}_2 = 2\left(G_{\langle m+1\rangle}J_3^{\langle m+1\rangle}\frac{1+v_{\langle m+1\rangle}}{1-v_{\langle m+1\rangle}}+\sum_{r=1}^{m}G_{\langle r\rangle}J_4^{\langle r\rangle}\frac{1+v_{\langle r\rangle}}{1-v_{\langle r\rangle}}\right)$$

$$\mathscr{L}_1 = -\frac{2}{3}\left[A_{(m+1)}\frac{G_{\langle m+1\rangle}}{G'_{\langle m+1\rangle}}h_{m+1}^3+\sum_{r=1}^{m}A_{(r)}\frac{G_{\langle r\rangle}}{G'_{\langle r\rangle}}(h_r^3-h_{r-1}^3)\right]$$

$$\mathscr{L}_2 = -\frac{2}{3}\left[A_{(m+1)}\frac{G_{m+1}}{G'_{\langle m+1\rangle}}\frac{1+v_{\langle m+1\rangle}}{1-v_{\langle m+1\rangle}}h_{m+1}^3 + \sum_{r=1}^{m} A_{(r)}\frac{G_{\langle r\rangle}}{G'_{\langle r\rangle}}\frac{1+v_{\langle r\rangle}}{1-v_{\langle r\rangle}}(h_r^3 - h_{r-1}^3)\right]$$

$$\mathscr{S}_1 = \sum_{r=1}^{m} G_{\langle r\rangle}\Omega_{(r)}(h_r^2 - h_{r-1}^2)$$

$$\mathscr{S}_2 = \sum_{r=1}^{m} G_{\langle r\rangle}\Omega_{(r)}\frac{1+v_{\langle r\rangle}}{1-v_{\langle r\rangle}}(h_r^2 - h_{r-1}^2).$$

## Appendix 3: Expressions of the stiffness quantities associated with Model I

$$B \equiv \frac{1}{3}\left[\bar{E}_{\langle m+1\rangle}(1+v_{\langle m+1\rangle})h_{m+1}^3 + \sum_{r=1}^{m}\bar{E}_{\langle r\rangle}(1+v_{\langle r\rangle})(h_r^3 - h_{r+1}^3)\right]$$

$$C \equiv \frac{1}{3}\left[\bar{E}_{\langle m+1\rangle}(1+v_{\langle m+1\rangle})h_{m+1}^3 + \sum_{r=1}^{m}\bar{E}_{\langle r\rangle}(1-v_{\langle r\rangle})(h_r^3 - h_{r+1}^3)\right]$$

$$\mathscr{D} \equiv \frac{2}{3}\left[\bar{E}_{\langle m+1\rangle}h_{m+1}^3 + \sum_{r=1}^{m}\bar{E}_{\langle r\rangle}(h_r^3 - h_{r+1}^3)\right]$$

$$S \equiv 2G'_{\langle m+1\rangle}h_{m+1} + 2\sum_{r=1}^{m} G'_{\langle r\rangle}(h_r - h_{r-1}).$$

Herein and in the previously displayed equations

$$\bar{E} \equiv \frac{E}{1-v^2}.$$

## References

Amazigo, J.C., Budiansky, B., Carrier, G.F., 1970. Asymptotic analyses of the buckling of imperfect columns on nonlinear elastic foundations. International Journal of Solids and Structures 6, 1341–1356.

Ambartsumian, S.A., 1967. The Theory of Anisotropic Plates (in Russian). Nauka, Moscow.

Carrera, E. 1996. $C^0$ Reissner-Mindlin multilayered plate elements including zig-zag and interlaminar stress continuity. International Journal of Numerical Methods in Engineering 39, 1797–1820.

Carrera, E., Kroplin, B.H., 1997. Zig-zag and interlaminar equilibria effects in large deflection and postbuckling analysis of multilayered plates. Mechanics of Composite Material and Structures 4, 89–94.

Carrera, E., 1998. Evaluation of layerwise mixed theoreis for laminated plates analysis. AIAA Journal 36 (5), 830–839.

Cheng, Z.-Q., Jemah, A.K., Williams, F.W., 1996. Theory for multilayered anisotropic plates with weakened interfaces. Journal of Appl. Mechanics, Trans. ASME 63, 1019–1026.

Cheng, Z.-Q., Kennedy, D., Williams, F.W., 1996. Effect of interfacial imperfection on buckling and bending behavior of composite laminates. AIAA Journal 34, 12.

Cheng, Z.-Q., Howson, W.P., Williams, F.W., 1997. Modeling of weakly bonded laminated composite plates at large deflections. International Journal of Solids and Structures 34 (27), 3583–3599.

Chattopadhyay, A., Gu, H., 1994. A new higher-order plate theory in the modeling delamination buckling of composite laminates. AIAA Journal 32 (8), 1709–1718.

Chattopadhyay, A., Gu, H., 1996a. Elasticity solution for delamination buckling of composite plates. Pre. 37th AIAA/ASME/ASCE/AHS/ASC Structures, Structural Dynamics and Materials Conf. Salt Lake City, UT, April 1996.

Chattopadhyay, A., Gu, H., 1996b. An experimental investigation of delamination buckling and postbuckling of composite laminates. Proceedings ASME Int. Mech. Eng. Congress and Exposition, Atlanta, GA, November, 1996.

Di Sciuva, M., 1992. Multilayered anisotropic plate models with continuous interlaminar stresses. Composite Structures 22, 149–164.

Di Sciuva, M., 1997. A geometrically nonlinear theory of multilayered plates with interlayer slips. AIAA Journal 35 (11), 7, 1753–1759.

Di Sciuva, M., Icardi, U., 1996. On modeling of global response behavior of sandwich plates with laminated faces. In: Topping, B.H.V. (Ed.), Advances in Analysis and Design of Composites. Civil Comp. Press, Edinburgh, Scotland B6/25.

Di Sciuva, M., Icardi, U., Librescu, L., 1997. On modeling of laminated composite structures featuring interlaminae imperfections. In: Predeleanu, M., Gilormini, P. (Eds.), Advanced Methods in Materials Processing Defects. Studies in Applied Mechanics, Vol. 45. Elsevier, Amsterdam, pp. 395–403.

Green, A.E., Zerna, W., 1968. Theoretical Elasticity. Clarendon Press, Oxford.

He, L.H., 1995. Non-linear theory of laminated shells accounting for continuity conditions of displacements and tractions at layer interfaces. Int. J. Mech. Sci. 37 (2) 161–173.

Icardi, U., Librescu, L., Di Sciuva, M., 1997. Thermomechanical response of laminated flat panels featuring interlaminae bonding imperfections. In: Simitses, G.J. (Ed.), Analysis and Design Issues for Modern Aerospace Vehicles, AD-Vol. 55. ASME, New York, NY 10017, pp. 197–214.

Librescu, L., 1975. Elastostatics and Kinetics of Anisotropic and Heterogeneous Shell-Type Structures. Noordhoff Internat. Publ., Leyden, The Netherlands.

Librescu, L., 1987. Refined geometrically non-linear theories of anisotropic laminated shells. Quarterly of Applied Mathematics 45, 1–22.

Librescu, L., Chang, M.-Y., 1992. Postbuckling and imperfection sensitivity of shear deformable composite double-curved panels. International Journal of Solids and Structures, 29 (9), 1065–1083.

Librescu, L., Chang, M.-Y. 1993. Effects of geometric imperfections on vibration of compressed shear deformable laminated composite curved panels. Acta Mechanica 96, 203–224.

Librescu, L., Lin, W., 1996. Two models of shear deformable laminated plates and shells and their use in prediction of global response behavior. European Journal of Mechanics, A/Solids 15 (6), 1095–1120.

Librescu, L., Lin, W., 1996. Thermomechanical postbuckling and plates and shells incorporating non-classical effects. In: Hetnarski, R.B. (Ed.), Thermal Stresses IV. Elsevier, Amsterdam, pp. 103–179.

Librescu, L., Lin, W., 1997a. Vibration of thermomechanically loaded flat and curved panels taking into account geometric imperfections and tangential edge restraint. International Journal of Solids and Structures 34 (17), 2161–2181.

Librescu, L., Lin, W., 1997b. Postbuckling and vibration of shear deformable flat and curved panels on nonlinear elastic foundation. International Journal of Non-Linear Mechanics 32 (2), 211–225.

Librescu, L., Reddy, J.N., 1986. A critical evaluation and generalization of the theory of anisotropic laminated composite panels. Proceedings of the American Society for Composites, First Technical Conference, Technonic Publ. Co. Inc. Lancaster, Basel, pp. 473–489.

Librescu, L., Schmidt, R., 1991. Substantiation of a shear-deformable theory of anisotropic composite laminated shells accounting for the interlaminae continuity conditions. International Journal of Engineering Science 29, 669–683.

Librescu, L., Stein, M., 1991. A geometrically nonlinear theory of transversely-isotropic laminated composite plates and its use in the post-buckling analysis. Thin-Walled Structures, Special Aerospace Structures Issue 11, pp. 177–201.

Librescu, L., Lin, W., Di Sciuva, M., Icardi, U., 1997. Postbuckling of laminated composite and sandwich plates and shells: on the significance of the fulfilment of static interlayer continuity conditions. Computer Methods Appl. Mech. Engr. 148, 165–186.

Librescu, L., Lin, W., Nemeth, M.P., Starnes Jr, J.H., 1993. Classical versus non-classical postbuckling behavior of laminated composite panels under complex loading conditions. In: Librescu, L. (Ed.), Non-Classical Problems of

the Theory and Behavior of Structures Exposed to Complex Environmental Conditions. AMD-Vol. '164, ASME, pp. 169–182.

Librescu, L., Lin, W., Nemeth, M.P., Starnes Jr, J.H., 1994. Effects of a thermal field on frequency–load interaction and geometrically imperfect shallow curved panels. Paper AIAA-94-1342, AIAA/ASME/ASCE/AHS/ASC 35th Structures, Structural Dynamics, and Material Conference, Hilton Head, SC.

Librescu, L., Lin, W., Nemeth, M.P., Starnes Jr, J.H., 1995. Thermomechanical postbuckling of geometrically imperfect flat and curved panels taking into account tangential edge constraints. Journal of Thermal Stresses 8 (4), 465–482.

Librescu, L., Lin, W., Nemeth, M.P., Starnes Jr, J.H., 1996. Frequency–load interaction of geometrically imperfect curved panels subjected to heating. AIAA Journal 34 (1) 166–177.

Librescu, L., Lin, W., Nemeth, M.P., Starnes Jr, J.H., 1996b. Vibration of geometrically imperfect panels subjected to thermal and mechanical loads. Journal of Spacecraft and Rockets 33 (2), 285–291.

Malvern, L.E., 1969. Introduction to the Mechanics of a Continuous Medium. Prentice-Hall, Englewood Cliffs, NJ.

Naghdi, P.M., 1963. Foundation of elastic shell theory. In: Sneddon, L.N., Hill, R. (Eds.), Progress of Solid Mechanics, Vol. 1. North-Holland, Amsterdam, p. 1.

Noor, A.K., Burton, W.S., 1990. Assessment of computational models for multilayered composite shells. Appl. Mech. Revs 43, 67–97.

Noor, A.K., Burton, W.S., 1992. Computational models of high-temperature multilayered composite plates and shells. Appl. Mech. Revs 45 (10), 414–446.

Pai, P.F., Nayfeh, A.H., 1994. A unified nonlinear formulation for plate and shell theories. Nonlinear Dynamics 6, 459–500.

Reddy, J.N., Robbins Jr, D.H., 1994. Theories and computational models for composite laminates. Appl. Mech. Revs 47, 147–169.

Schmidt, R., Librescu, L., 1994. Further results considering the refined theory of anisotropic laminated composite plates. Journal of Engineering Mathematics 28, 407–425.

Schmidt, R., Librescu, L., 1996. Geometric nonlinear theory of laminated anisotropic composite plates featuring interlayer slips. Nova Journal of Mathematics, Game Theory and Algebra 5 (2), 131–147.

Seide, P., 1974. A re-examination of Koiter's theory of initial postbuckling behavior and imperfection sensitivity of structures. In: Fung, C.Y., Sechler, E.E. (Eds.), Thin Shell Structures: Theory, Experiment and Design. Prentice-Hall, NJ, pp. 59–80.

Simitses, G.J., 1986. Buckling and postbuckling of imperfect cylindrical shells: a review. Appl. Mech. Revs 39 (10), 1517–1524.

Timarci, T., Soldatos, K.P. 1995. Comparative dynamic studies for symmetric cross-ply circular cylindrical shells on the basis of a unified shear deformable shell theory. Journal Sound and Vibration 18, 602–624.

Volmir, A.S., 1967. Stability of Deformable Systems (in Russian). Nauka, Moscow.

Woods, R.H., 1976. Pyrolytic graphite for high pressure, high temperature applications. AIAA Paper pp. 76–605.

Xavier, P.B., Chew, C.H., Lee, K.H., 1995. Buckling and vibration of multilayered orthotropic composite shells using a simple higher-order layerwise theory. International Journal of Solids and Structures 32 (23), 3479–3497.